

# Extreme Value Analysis for Finite, Multivariate and Correlated Systems with Finance as an Example

Benjamin Köhler, Anton J. Heckens, and Thomas Guhr

*Fakultät für Physik, Universität Duisburg–Essen, Duisburg, Germany*

## Abstract

Extreme values and the tail behavior of probability distributions are essential for quantifying and mitigating risk in complex systems of all kinds. In multivariate settings, accounting for correlations is crucial. Although extreme value analysis for infinite correlated systems remains an open challenge, we propose a practical framework for handling a large but finite number of correlated time series. We develop our approach for finance as a concrete example but emphasize its generality. We study the extremal behavior of high-frequency stock returns after rotating them into the eigenbasis of the correlation matrix. This separates and extracts various collective effects, including information on the correlated market as a whole and on correlated sectoral behavior from idiosyncratic features, while allowing us to use univariate tools of extreme value analysis. This holds even for high-frequency data where discretization effects normally complicate analysis. We employ a peaks-over-threshold approach and thereby fully avoid the analysis of block maxima. We estimate the tail shape of the rotated returns while explicitly accounting for nonstationarity, a key feature in finance and many other complex systems. Our framework facilitates tail risk estimation relative to larger trends and intraday seasonalities at both market and sectoral levels.

## 1 Introduction

Estimating properties of rare and extreme events, such as their magnitude, frequency and temporal dynamics is crucial for understanding systemic stability as well as for managing and mitigating risk in complex systems, ranging from weather, climate and hydrology to socio-economic systems such as traffic, social insurance and financial markets [1–6]. Complex systems often exhibit significant correlations, both in the time domain as well as over different system constituents. In finance, the latter gave rise to the method of diversification and Markowitz’ famous Portfolio optimization [7]. Long range dependency in absolute values of financial returns is well-established, see for instance Refs. [8, 9]. In addition, nonstationarity is typically a key feature, since system dynamics often change drastically and extreme events such as market crashes occur [10, 11]. Recent empirical and analytical studies have shown that in general, fluctuations of correlations between stock returns lift the tails of the

---

*Email addresses:* benjamin.koehler@uni-due.de (Benjamin Köhler), anton.heckens@uni-due.de (Anton J. Heckens), thomas.guhr@uni-due.de (Thomas Guhr)

multivariate return distributions [12–14]. Thus analysis without an adequate handling of dependencies and using tools which rely on stationarity might lead to false risk assessment, in the worst cases to considerable underestimation of risk [15, 16].

The key theorems of extreme value theory for univariate time series were first derived by Fisher and Tippett [17] and formalized by Gnedenko [18]. Decades later, the mathematically equivalent description of extremal limit distributions arising from excess distributions was pioneered by Balkema, de-Haan [19] and Pickands [20]. The field is application-driven and interdisciplinary in nature. Some areas where even early extreme value theory proved useful for empirical analysis, are hydrology, especially flood research, meteorology and material science [21–23]. Since then various fields have influenced mathematical research on a more general understanding of extreme values. All these results apply to the univariate case.

Extreme value theory for correlated systems has been studied in detail [24, 25], with a focus on autocorrelations in a single time series, *i.e.* in a univariate setting. Here we address an issue of conceptual and practical interest, namely extreme value statistics for a large, but finite number of cross-dependent time series, whose mutual bilinear statistical dependencies are captured by a Pearson correlation matrix. However, the measure of mutual dependencies is not limited to linear correlation measures, nonlinear measures such as tail-dependence matrices are also relevant. The goal of this paper is to address the following four points:

- Develop a framework for analyzing extreme values in multivariate, highly correlated time series, using tools from univariate extreme value statistics while still capturing properties of the full correlated system.
- Introduce and motivate the rotation into the eigenbasis of the correlation matrix as a practical way to handle dependence and to identify collectivity.
- Apply a threshold-based approach, which naturally yields tail behavior as well as extreme value statistics. This allows us to avoid common, but rather arbitrary block maxima approaches.
- Discuss how to account for nonstationarity and what this implies for our method.

To be concrete, we use finance as an example and carry out an extreme value analysis of empirical data from the New York Stock Exchange (NYSE) for the year 2014 at an intraday resolution level. We apply a method focusing on the tail behavior of the marginal distributions, *i.e.* the tail behavior without accounting for seasonality and nonstationarity, and compare with the results of our new method incorporating intraday volatility clustering and nonstationarity. Our approach allows analyzing high-frequency returns on a timescale of seconds.

In Sec. 2, the aim is to give a short and certainly non exhaustive introduction to extreme value analysis, regarding independent as well as weakly serial dependent random variables. In Sec. 3 we introduce our estimation methods, as well as the data set and data transformation. We describe the rotation of the returns and investigate the interpretation of these rotated returns in Sec. 4. Finally, Sec. 5 portrays the main results of our analysis, conclusions are given in Sec. 6.

## 2 Univariate Extreme Value Theory

This short depiction of extreme value theory (EVT) is mainly based on Refs. [26, 27]. We focus on maxima, but the theory is derived analogously for minima. In Sec 2.1, we summarize the basic theory for stationary, independent and identically distributed series of random variables. In Sec. 2.2 we deal with the generalization to processes with serial dependence, that is dependence of the random variables in time and in Sec. 2.3 we briefly describe the extremal index.

Importantly, we afterwards study a finite, multivariate and correlated system, in our data analysis. There are methods of multivariate extreme value analysis for time series analysis, which can be found for instance in Ref. [26]. However, we provide a new method of analyzing such a system, relying solely on basic univariate EVT and we prove its usefulness for our application.

### 2.1 Independent Random Variables

The Fisher-Tippett-Gnedenko theorem [17, 18] addresses the maxima of a univariate series  $(X_i)_{i \in \mathbb{N}}$  of independent and identically distributed (i.i.d.) random variables. It states that if there are series of rescaling constants  $a_n \in \mathbb{R}_{>0}$ ,  $b_n \in \mathbb{R}$ , so that the limit of the cumulative distribution function of  $(\max_{i=1, \dots, n} X_i - b_n)/a_n$  exists then it is one of three types of distributions. Mathematically, the cumulative distribution function can be found as

$$\begin{aligned} \mathbb{P}\left(\frac{\max_{i=1, \dots, n} X_i - b_n}{a_n} \leq x\right) &= \mathbb{P}\left(\bigcap_{i=1, \dots, n} \{X_i \leq a_n x + b_n\}\right) \\ &= \prod_{i=1}^n \mathbb{P}(X_i \leq a_n x + b_n) = F^n(a_n x + b_n), \end{aligned} \quad (1)$$

where the second and the third equality signs follow from independence and identity of distribution, respectively. The theorem now states that if  $\lim_{n \rightarrow \infty} F^n(a_n x + b_n)$  exists in a nondegenerate way, then

$$\lim_{n \rightarrow \infty} F^n(x) = G_{\gamma, b, a}^{\text{EV}}(x) = \begin{cases} \exp\left(-\left(1 + \gamma\left(\frac{x-b}{a}\right)\right)^{-1/\gamma}\right), & \gamma \in \mathbb{R} \setminus \{0\} \\ \exp\left(-\exp\left(-\frac{x-b}{a}\right)\right), & \gamma = 0 \end{cases} \quad (2)$$

with constants  $a \in \mathbb{R}_{>0}$ ,  $b \in \mathbb{R}$ . The most relevant parameter is  $\gamma$ , since it distinguishes the three fundamental types of behavior of extreme values. The cumulative distribution is of Gumbel, Fréchet or Weibull type for  $\gamma = 0$ ,  $\gamma > 0$  and  $\gamma < 0$ , respectively. The corresponding probability density function reads

$$g_{\gamma, b, a}^{\text{EV}}(x) = \frac{1}{a} \begin{cases} \left(1 + \gamma\left(\frac{x-b}{a}\right)\right)^{-1+1/\gamma} \exp\left(-\left(1 + \gamma\left(\frac{x-b}{a}\right)\right)^{-1/\gamma}\right), & \gamma \in \mathbb{R} \setminus \{0\} \\ \exp\left(-\frac{x-b}{a}\right) \exp\left(-\exp\left(-\frac{x-b}{a}\right)\right), & \gamma = 0 \end{cases} \quad (3)$$

and is depicted in Fig. 1. While the Gumbel distribution has unbounded support on the real axis and decays exponentially in the tails, the Fréchet distribution has a fixed lower limit and

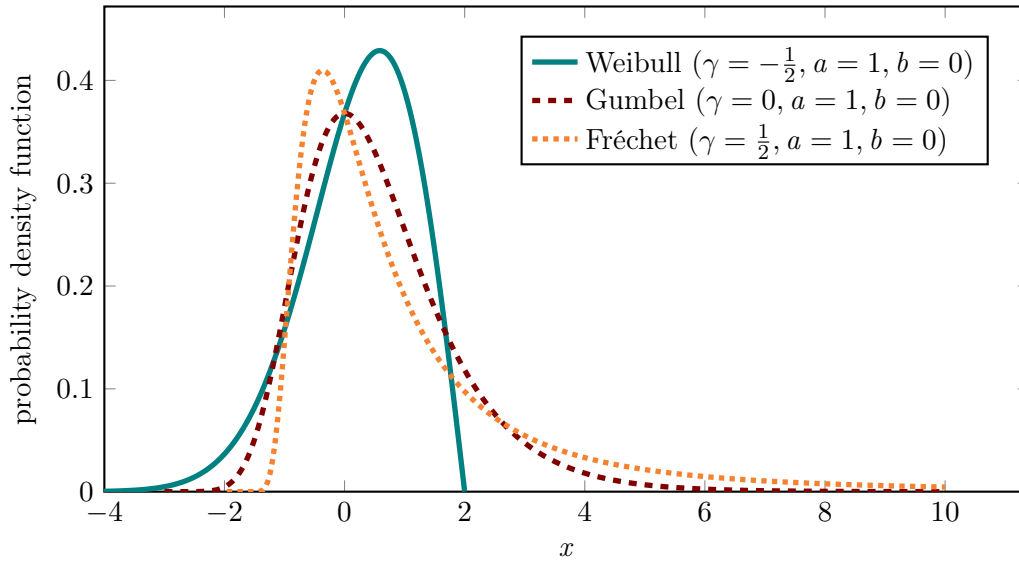


Figure 1: Probability density function  $g_{\gamma, b, a}^{\text{EV}}(x)$  for  $\gamma = 0$  and special cases  $\gamma = -1/2 < 0, \gamma = 1/2 > 0$ .

describes a power law decay in the upper tail. On the other hand, the Weibull distribution has an upper limit and a power law in its lower tail. Importantly the series  $a_n, b_n$  are not necessarily unique. If an underlying cumulative distribution  $F$  is known there are however strategies to calculate specific series if they exist, see for instance Ref. [24].

The common method to analyze extreme value behavior in measured data is the block maxima (BM) approach. The time series is divided into blocks from which the maxima are extracted, and  $G_{\gamma, b, a}^{\text{EV}}$  is then fitted to the distribution of maxima. The parameters  $\gamma$  and the appropriate rescaling in the limit  $a, b$  are typically estimated from the fit. For an exemplary application of the BM approach in a financial setting, see Ref. [28].

The Pickands–Balkema–DeHaan theorem [19, 20] paves the road for a quite different method of analysis. The focus is on the whole tail of the marginal probability distribution for a series of i.i.d. random variables. We look at the cumulative conditional excess distribution function, defined as

$$F_u(x) = \mathbb{P}(X - u \leq x \mid X > u) = \frac{F(x + u) - F(u)}{1 - F(u)}. \quad (4)$$

It describes the cumulative distribution of random variables, conditioned on their exceedance of a threshold  $u$ . The theorem states, that if there is an appropriate rescaling such that  $\lim_{n \rightarrow \infty} F^n(a_n x + b_n)$  exists as in the premise of the Fisher–Tippett–Gnedenko theorem, then

$$\lim_{u \rightarrow \infty} F_u(x) = G_{\gamma, \sigma}^{\text{GPD}}(x), \quad \text{where} \quad G_{\gamma, \sigma}^{\text{GPD}}(x) = \begin{cases} 1 - (1 + \frac{\gamma x}{\sigma})^{-1/\gamma}, & \gamma \in \mathbb{R} \setminus \{0\} \\ 1 - e^{-\frac{x}{\sigma}}, & \gamma = 0 \end{cases}. \quad (5)$$

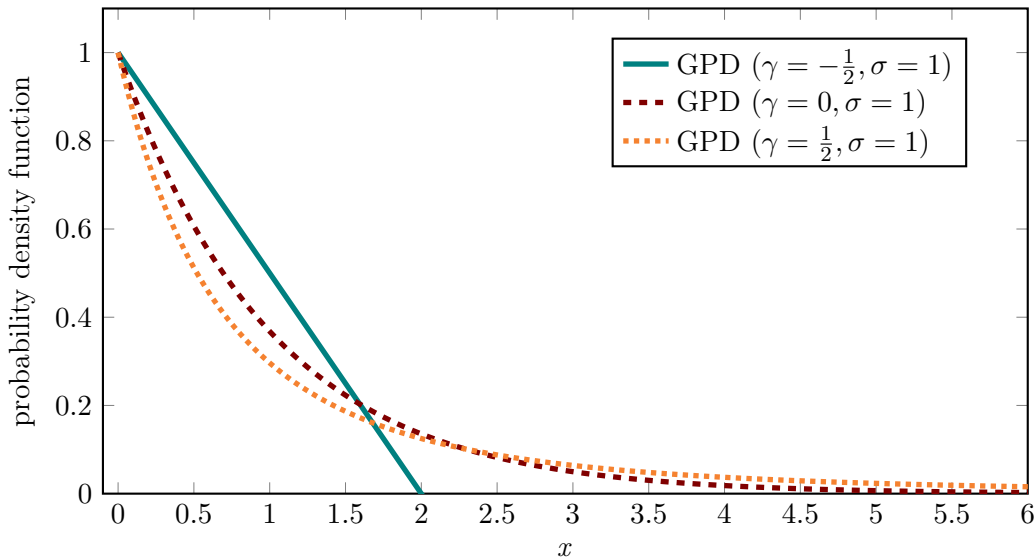


Figure 2: Probability density function  $g_{\gamma,\sigma}^{\text{GPD}}(x)$  for  $\gamma = 0$  and special cases  $\gamma = -1/2 < 0, \gamma = 1/2 > 0$ .

This family  $G_{\gamma,\sigma}^{\text{GPD}}$  is called the generalized Pareto distribution (GPD). The parameter  $\gamma$  is the same as in the family of extreme value distributions (2), while

$$\sigma = a + \gamma(u - b). \quad (6)$$

The corresponding probability density function reads

$$g_{\gamma,\sigma}^{\text{GPD}}(x) = \frac{1}{\sigma} \begin{cases} (1 + \frac{\gamma x}{\sigma})^{-1/\gamma-1}, & \gamma \in \mathbb{R} \setminus \{0\} \\ e^{-\frac{x}{\sigma}}, & \gamma = 0 \end{cases} \quad (7)$$

and is depicted in Fig. 2.

This result leads to another technique of empirically extracting extremal behavior, called the peaks-over-threshold (POT) approach. We choose a threshold  $u$  and estimate the parameters  $\gamma, \sigma$  from fitting  $G_{\gamma,\sigma}^{\text{GPD}}$  to the empirical cumulative conditional excess distribution function  $F_u^{\text{empirical}}(x)$ .

There are several practical advantages of the POT approach over the BM estimation [27]. While the latter takes into account only one data point in each block and discards the others, the former uses all exceedances over a certain threshold. Thus POT estimations often make more efficient use of the available data, which is crucial when dealing with extremes which are rare events and often leads to faster convergence in data analysis contexts. Due to the use of higher-order statistics instead of only first-order statistics, the POT approach is also arguably more intuitive in fields where not only the extremes but the whole tails of distributions are of general interest. Furthermore, although relying on a threshold, the POT are not tied to a certain block size in the time domain. Different block sizes can bias results differently, depending on the dynamics of the underlying process. For exemplary applications of POT we refer to Refs. [27, 29] and in particular regarding a financial setting to Ref. [30].

## 2.2 Dependent Processes

The findings for the independent case can be generalized to dependent, but still stationary series of random variables under two types of restrictions usually denoted as  $\mathbf{D}$  and  $\mathbf{D}'$  in the literature [31].

- The first condition  $\mathbf{D}$  is a *weak* mixing condition. For  $u_n = a_n x + b_n$ , there must be a counting sequence  $l_n = \mathcal{O}(n)$ , such that for the two sets of disjoint indices  $A \subset \{1, \dots, k\}$ ,  $B \subset \{k + l_n, \dots, n\}$  one has

$$\max_{A,B} \{|\mathbb{P}(X_i \leq u_n, i \in A \cup B) - \mathbb{P}(X_i \leq u_n, i \in A)\mathbb{P}(X_i \leq u_n, i \in B)|\} \xrightarrow{n \rightarrow \infty} 0.$$

In the independent case the above difference is zero by definition. For dependent processes this means that for growing distances between two disjoint sets of subsequent random variables, the random variables are decreasingly dependent on each other. This is a notion of long-range independence. In the physics literature a similar condition is often used, by stating that there is a finite correlation length beyond which the variables become uncorrelated, see for instance Ref. [25].

- The second, *stronger* mixing condition  $\mathbf{D}'$  prohibits short-range clustering,

$$\lim_{n \rightarrow \infty} \left( n \sum_{i=2}^{\lfloor n/k \rfloor} \mathbb{P}(X_1 > u_n, X_i > u_n) \right) \xrightarrow{k \rightarrow \infty} 0,$$

by restricting the joint probability of two extremes occurring in an ever shorter time window  $\lfloor n/k \rfloor$ . The sum accounts for all pairs in this time window.

If  $\mathbf{D}$  is satisfied, then in the limit of  $n \rightarrow \infty$ , the value of  $\gamma$  is the same as for a series of independent variables with the same marginal distribution and only the appropriate rescaling differs, see Ref. [31] and compare Ref. [27] for a more intuitive derivation in the Fisher–Tippett–Gnedenko setting. The key point is that one has to correctly estimate clustering of extremes in time. In empirical analysis, it is a standard approach to use declustering algorithms, where only the independent maxima of extremal clusters are used for analysis. However, in the mathematical limit both cumulative distributions, the one of the cluster maxima and the one of the clustered threshold exceedances converge to cumulative distributions with the same  $\gamma$  when  $\mathbf{D}$  is satisfied, see also the contribution of Anderson [32] in the discussion of Ref. [33]. Yet, to make use of this equivalence one has to assume stationarity after all. In intraday financial data, nonstationarity and serial dependence is clearly a factor, which will be relevant later on in Sec. 5.

Another important caveat, when applying the above results to real data, is that in order to use the result under condition  $\mathbf{D}$ , the degree of long-range serial dependence must be quantified carefully. A series may show no significant linear autocorrelations, but a nonlinear transformation may show autocorrelations and therefore the series is not independent. If these nonlinear autocorrelations are strongly persistent, above results may not be directly applicable in data analysis since  $\mathbf{D}$  is not satisfied. In this case, convergence to the theoretical distributions has to be thoroughly checked.

### 2.3 Extremal Index

If the stronger condition  $\mathbf{D}'$  is satisfied, even the rescaling is the same as in the i.i.d case, see Ref. [34]. However, for empirical time series of many systems, including finance,  $\mathbf{D}'$  is not satisfied and we have to resort to  $\mathbf{D}$  because short range clustering is apparent. The strength of this clustering is usually captured by the extremal index  $\Theta \in [0, 1]$ , which is defined as the inverse of the mean cluster size of extremes. We briefly sketch an intuitive interpretation of the extremal index. In addition we relate the index to the waiting times between exceedances. For more details, mathematically exact definitions and proofs, we refer to the literature, for instance Refs. [34–36]. Given the total number of threshold exceedances  $n$ , the number of independent clusters of exceedances  $n_C$  is approximately

$$n_C \approx n\Theta, \quad (8)$$

where  $\Theta$  is the inverse mean cluster size. The probability of  $X_i$  exceeding  $u$  is  $1 - F(u)$ . An exceedance falls into a cluster with probability  $1 - \Theta$ , but different clusters are independent of each other. Either the exceedance falls into a cluster, then a rescaled waiting time  $w$  is zero, or it starts a new cluster and is independent from previous observations, then  $w$  is larger than zero. Thus, the waiting times between exceedances  $\tau_i$  rescaled with the probability of exceeding the threshold follow the probability density function [36]

$$\lim_{u \rightarrow \infty} \mathbb{P}(\tau_i(1 - F(u)) = w) = \begin{cases} 1 - \Theta, & w = 0 \\ \Theta \text{Exp}(\Theta), & w > 0 \end{cases}, \quad (9)$$

where  $\text{Exp}(\Theta)$  denotes the probability density function of the exponential distribution with mean  $1/\Theta$ . In the case  $\Theta = 1$ , we retain the pure exponential density of waiting times, as expected for a Poisson process, there is no clustering. If we calculate the first two moments of the distribution of  $\tau_i$  itself from (9), we find

$$\mathbb{E}[\tau_i] = \frac{1}{1 - F(u)}, \quad \mathbb{E}[\tau_i^2] = \frac{2}{\Theta(1 - F(u))^2}, \quad (10)$$

and thus the identity [36]

$$\Theta = \frac{2(\mathbb{E}[\tau_i])^2}{\mathbb{E}[\tau_i^2]} \quad (11)$$

follows which only involves the first two moments of the waiting time distribution between exceedances.

## 3 Data Processing and Methods of Analysis

In Sec. 3.1 we describe our data and processing methods. We provide the statistical estimators and methods of estimation for the tail index  $\gamma$  and the extremal index  $\Theta$  in Sec. 3.2.

### 3.1 Processing the Data

Our data consists of time series obtained for  $K$  stocks from the Daily TAQ (Trade and Quote) files of the NYSE (New York Stock Exchange) in 2014. We choose an amount of  $K = 479$  liquid stocks from the S&P500. The smallest provided time resolution is 1 ms, we choose a resolution of seconds for our analysis. Since market dynamics shortly after the opening and shortly before closing differ significantly from the main trading phase, we discard the first ten and last fifteen minutes of each trading day. Especially in the phase of the closing auction, dissemination of the closing auction order imbalance leads to frequent sharp and large spikes in volatility and volume [37], which are only visible at high frequency. In the year 2014, the NYSE started this dissemination at 15:45:00 [38], therefore we exclude the trading phase after this time. For one full trading day we end up with  $T_{\text{day}} = 21899$  seconds of data. The early closing days of 24/12/2014, 28/11/2014, 03/07/2014 (dd/mm/Y) are removed completely, so that we end up with  $N_{\text{days}} = 248$  full trading days in 2014. This leaves us with a total amount of  $T = N_{\text{days}} T_{\text{day}} = 5430952$  seconds per stock.

Since trading is sometimes sparse at this high resolution, we construct the midpoint price for all stocks  $k$  and all times  $t$  by averaging best bid  $b_k$  and best ask  $a_k$  in the order book,

$$m_k(t) = \frac{a_k(t) + b_k(t)}{2}, \quad k = 1, \dots, K, \quad (12)$$

and use the last available midpoint price in each second  $t$ . When no bids or asks are available in one second, midpoint prices are estimated as the last existing midpoint price in time. From this, we calculate the logarithmic returns

$$G_k(t, \Delta t) = \ln m_k(t + \Delta t) - \ln m_k(t) = \ln \frac{m_k(t + \Delta t)}{m_k(t)}, \quad (13)$$

for all  $k$  and  $t$ , where we denote the return horizon with  $\Delta t$ . We restrict ourselves to intraday trading, thus overnight jumps in price are not included as returns. After arranging the return time series as rows of the  $K \times T$  data matrix  $G$ , we normalize the time series to zero mean and standard deviation of unity

$$M_k(t) = \frac{G_k(t) - \langle G_k(t) \rangle_t}{\sigma_k}, \quad (14)$$

where  $\langle G_k(t) \rangle_t$  and  $\sigma_k^2 = \text{var}_t(G_k(t))$  are sample mean and variance.

### 3.2 Estimation Procedure

For the estimation of the mean inverse cluster size  $\Theta$  we use the method described by Ferro and Segers [36]. The estimator  $\hat{\Theta}$  is related to the quotient of the square of the first moment and the second moment of the empirical distribution of the  $\tau_i$  according to

$$\hat{\Theta} = \begin{cases} \min \left( \frac{2 \langle (\tau_i - 1) \rangle_i^2}{\langle (\tau_i - 1)(\tau_i - 2) \rangle_i}, 1 \right), & \max \tau_i > 2 \\ \min \left( \frac{2 \langle (\tau_i) \rangle_i^2}{\langle \tau_i^2 \rangle_i}, 1 \right), & \max \tau_i \leq 2 \end{cases}, \quad (15)$$

where  $\langle \cdot \rangle_i$  indicates an average over all  $n - 1$  time spans  $\tau_i$ . This is the estimator version of Eq. (11), which we motivated already in Sec. 2.3. In the case of a perfect Poisson process  $\hat{\Theta}$  evaluates to 1, while for clustered exceedances it is smaller and scales with the real mean inverse cluster size  $\Theta$  of the process. The smaller  $\Theta$ , the larger is the average cluster of exceedances generated by the process. This is schematically depicted in Fig. 3.

To evaluate the tail behavior we use Maximum-Likelihood estimation for the parameters of the generalized Pareto distribution (5) of the peaks exceeding a certain threshold. Figure 4 shows a schematic depiction of the procedure. The log-likelihood of  $G_{\gamma, \sigma}^{\text{GPD}}$ , reads

$$l(\gamma, \sigma) = \begin{cases} -n \ln \sigma - \left(1 + \frac{1}{\gamma}\right) \sum_{i=1}^n \ln\left(1 + \gamma \frac{x_i}{\sigma}\right), & \text{for } \gamma \neq 0 \\ -n \ln \sigma - \sum_{i=1}^n \frac{x_i}{\sigma}, & \text{for } \gamma = 0 \end{cases}, \quad (16)$$

this function is maximized to obtain  $\hat{\gamma}$  and  $\hat{\sigma}$ . From Eq. (16), asymptotic variances as the squared standard errors of  $\hat{\gamma}$  and  $\hat{\sigma}$  are obtained in the context of the Fisher information matrix by Smith [39] as

$$\text{var}(\hat{\gamma}) \sim \frac{1}{n}(1 + \gamma)^2, \quad \text{var}(\hat{\sigma}) \sim \frac{1}{n}2\sigma^2(1 + \gamma). \quad (17)$$

They are accessibly provided in Ref. [29]. To evaluate the bias or goodness-of-fit we use the normalized root mean square deviation (NRMSD) related to quantile-quantile (Q-Q) plots. These are plots of the sorted time series  $\{x_i\}_{i=1, \dots, n}$  of peaks over threshold  $u$  against  $G_{\hat{\gamma}, \hat{\sigma}}^{\text{GPD}-1}\left(F_u^{\text{empirical}}(x_i)\right)$ , so we plot the empirical observations against the theoretically implied quantiles. If the estimated distribution were a perfect fit, we should see a straight line. The NRMSD as deviation from the straight line is calculated as

$$\rho = \frac{1}{\max_i(x_i) - \min_i(x_i)} \sqrt{\frac{1}{n} \sum_{i=1}^n \left(G_{\hat{\gamma}, \hat{\sigma}}^{\text{GPD}-1}\left(F_u^{\text{empirical}}(x_i)\right) - x_i\right)^2}. \quad (18)$$

Due to the bias-variance trade-off, the expected behavior of  $\rho$  is nonmonotonic. As the threshold  $u$  increases, the fit of the generalized Pareto distribution improves because the model becomes more appropriate for increasingly extreme data, leading to a decrease in  $\rho$ . However, beyond a certain threshold, the number of exceedances becomes too small which increases estimation variance and amplifies the influence of individual extreme observations. Therefore the fit loses quality and  $\rho$  increases again.

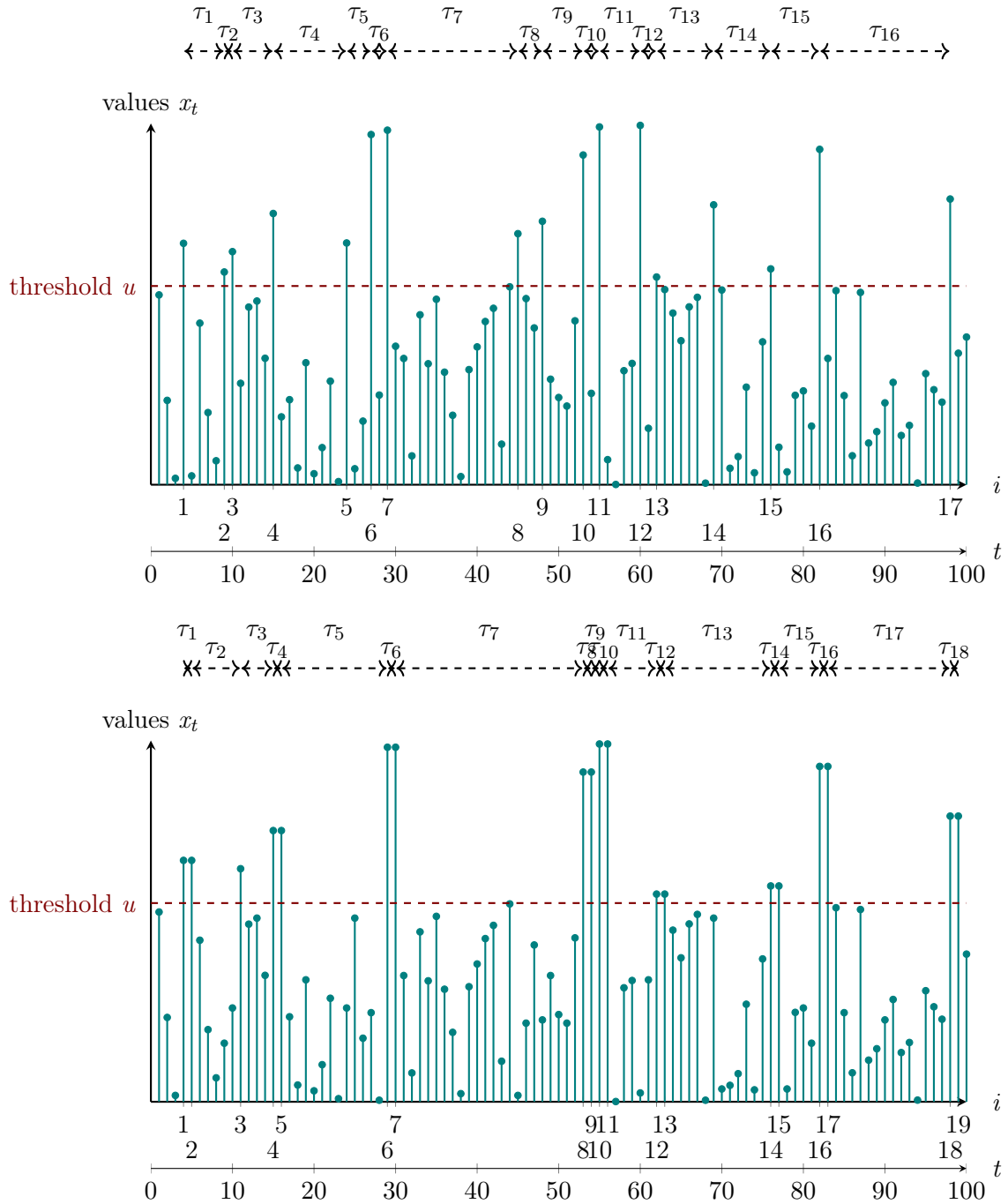


Figure 3: Schematic depiction of clustering of peaks over the threshold. Top: Independent, unclustered exceedances.  $\hat{\Theta} = 1$ . Bottom: Exceedances derived from the time series above, but occurring in clusters of two.  $\hat{\Theta} = 0.68$ .

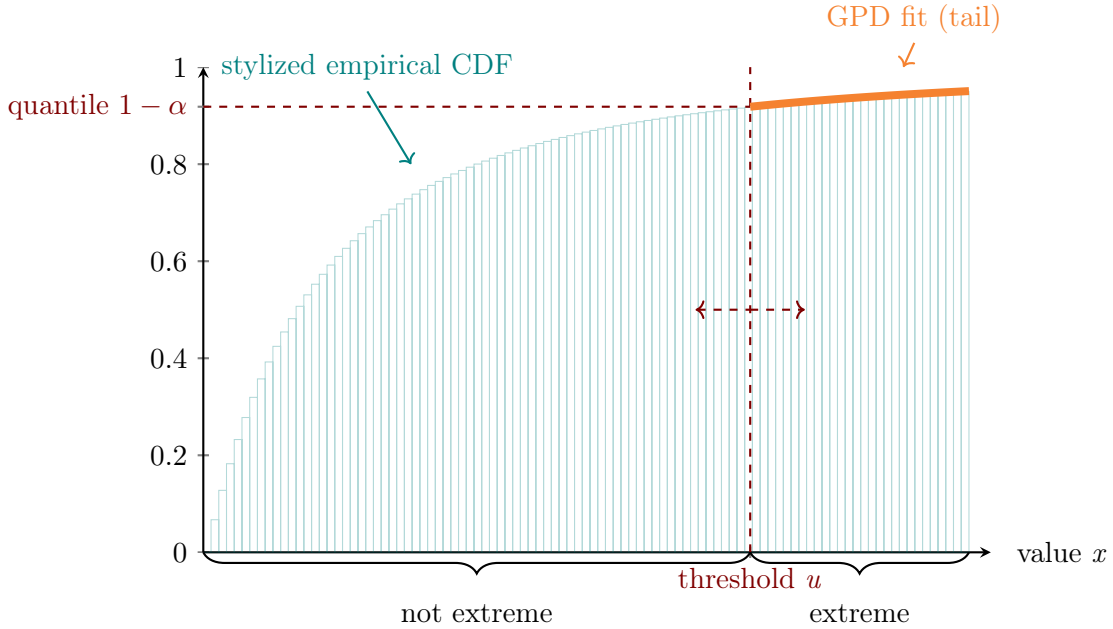


Figure 4: Schematic depiction of the estimation procedure.

## 4 Application to Multivariate Setting

Section 4.1 addresses the second point of the paper’s guiding questions: rotation into the eigenbasis of the correlation matrix. In Sec. 4.2 we shortly present the connection to portfolio risk management.

### 4.1 Rotated Returns

From the normalized data matrix we calculate a correlation matrix, with the Pearson correlation coefficient for each pair of stocks as its elements,

$$C = \frac{1}{T} MM^\dagger. \quad (19)$$

Since  $C$  is a symmetric, positive semidefinite matrix, the eigenvalues  $\Lambda_k, k = 1, \dots, K$ , are real and the diagonalizing matrices  $U, U^\dagger$  obtained from the spectral decomposition

$$C = U\Lambda U^\dagger, \quad \text{where} \quad \Lambda = \text{diag}(\Lambda_1, \dots, \Lambda_K), \quad (20)$$

are orthogonal. In our case  $C$  is positive definite. Random matrix theory suggests to interpret the large bulk in the eigenvalue density shown in Fig. 5 as random noise, while it is well known that the largest eigenvalue and its eigenvector encode information on the market as a whole [40]. The few smaller eigenvalues outside the bulk mainly correspond to industrial sectors, see Ref. [42] and Fig. 5 in the present contribution. We calculate the rotated and rescaled returns as

$$R = \Lambda^{-1/2} U^\dagger M, \quad (21)$$

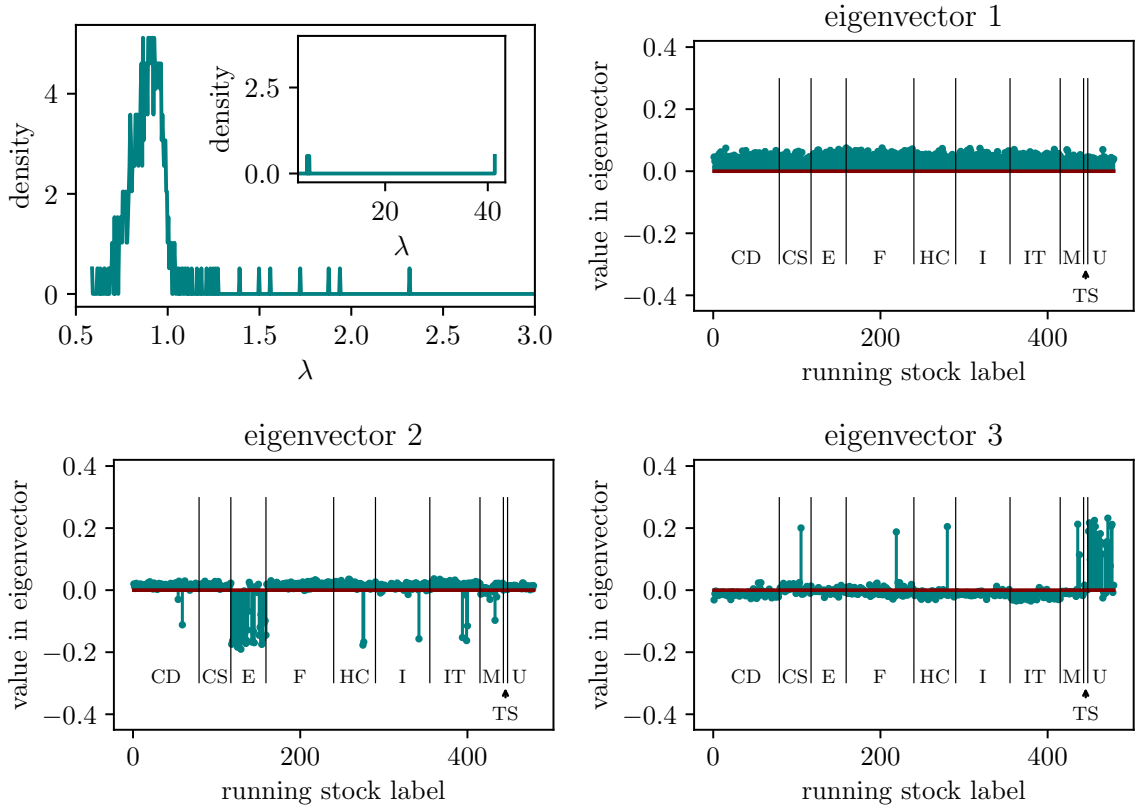


Figure 5: Top left: Spectral density of the financial correlation matrix ( $\Delta t = 1s$ ) of 2014. Top right and bottom: Largest three normalized eigenvectors visibly corresponding to the market, the Energy sector and the Utility sector of the GICS [41].

where we choose the positive sign when calculating the square root. By definition the  $\sqrt{\Lambda_k}$  are the standard deviations of the rotated time series  $(U^\dagger M)_k$ ,  $k = 1, \dots, K$ , thus  $R$  contains indeed rescaled and thus comparable time series  $R_k$  as its rows. In the statistics literature, this transformation (21) is usually called PCA-whitening [43], while in climate research this and similar approaches are often referred to as empirically orthogonal function (EOF) analyses. In climate research, these approaches are extensively used for reducing spatial dimensionality, see Ref. [44] as a typical and recent application. We refer to these rotated and rescaled time series as modes and number them according to the size of the eigenvalues, starting with the largest. The first thus reflects market behavior, while the second mode corresponds to the sector with the highest variance and so forth.

At small return horizons,  $\Delta t$  of 1s or comparable, the measurement of the correlation coefficients is influenced by the so-called Epps effect [45], and especially by tick-size discretization and asynchronicity effects [46–48]. Due to these effects, the correlation coefficients are decreasing with decreasing return horizon. Thus, when rotating into the eigenbasis (21), the Epps effect carries over to the multivariate analysis of returns. However, since the spectrum

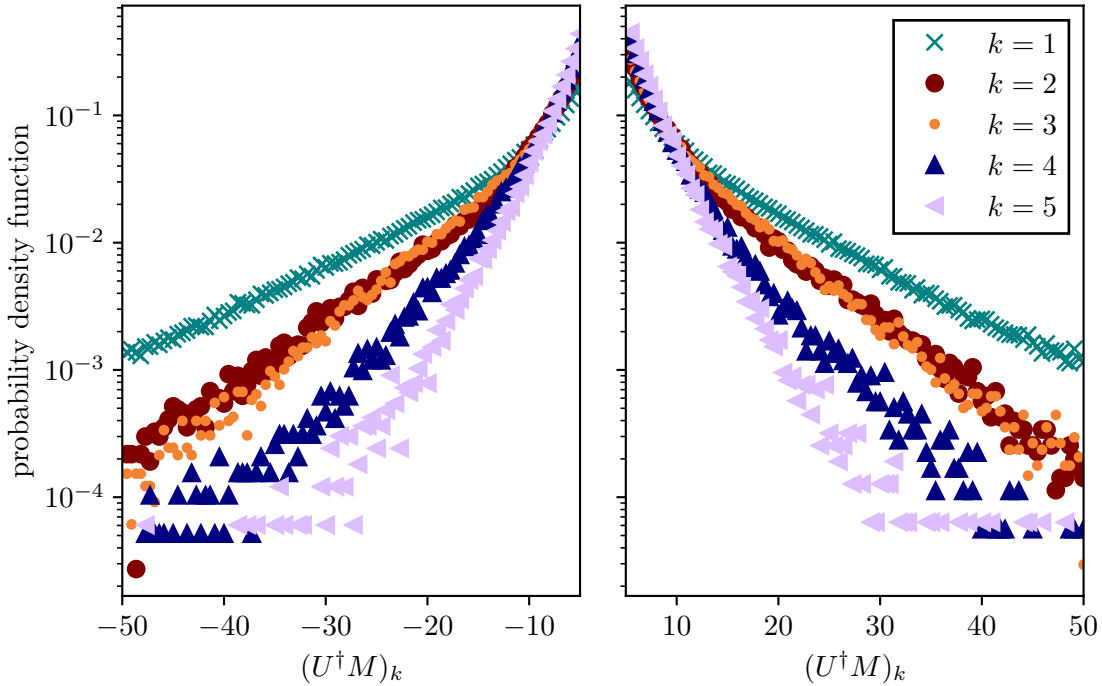


Figure 6: Left and right tails of the probability density functions for rotated returns referring to the five largest eigenvalues, without the rescaling  $1/\sqrt{\Lambda_k}$ .

of the correlation matrix  $C$  at  $\Delta t = 1$ s corresponds to meaningful eigenvectors, we do not correct for these effects here. The effect of tick size discretization is not only visible in the drop in correlation values, but also affects the marginal distributions of individual return time series, and thus an analysis of extreme value statistics at high frequencies. However the tick size affects different stocks differently. Thus due to the rotation, which is just a linear combination of return time series, the tick size effect is washed out, and the distributions appear smoothed, allowing for an extreme value analysis.

Regarding an in-depth analysis and a random matrix model for the multivariate distributions of the modes, we refer to Refs. [13, 14]. For the convenience of the reader, we briefly sketch relevant details here shortly. We see the influence of the rescaling  $\Lambda^{-1/2}$  from Eq. (21) in Figs. 6 and 7, where the tails of the probability densities for the rotated returns are plotted without and with the rescaling, respectively. In Fig. 7 we also plotted the aggregated probability density function, *i.e.* the density which emerges if we lump all  $R_k$  together. As explained in Ref. [14], this represents the average density referring to an eigenvalue of the bulk. This density was reproduced in Ref. [14] by a random matrix model, see Fig. 8. Figure 6 shows that the unscaled densities are ordered in accordance to the magnitude of the eigenvalues, while the rescaling in Fig. 7 removes this variance ordering. The densities are still not exactly the same, however the reason now is not the variance but the pure tail behavior, thus the ordering is now changed. Interestingly, in the range relevant for extreme values of the first five modes  $5 \lesssim |R_k| \lesssim 20$ , we notice that the aggregated density mostly

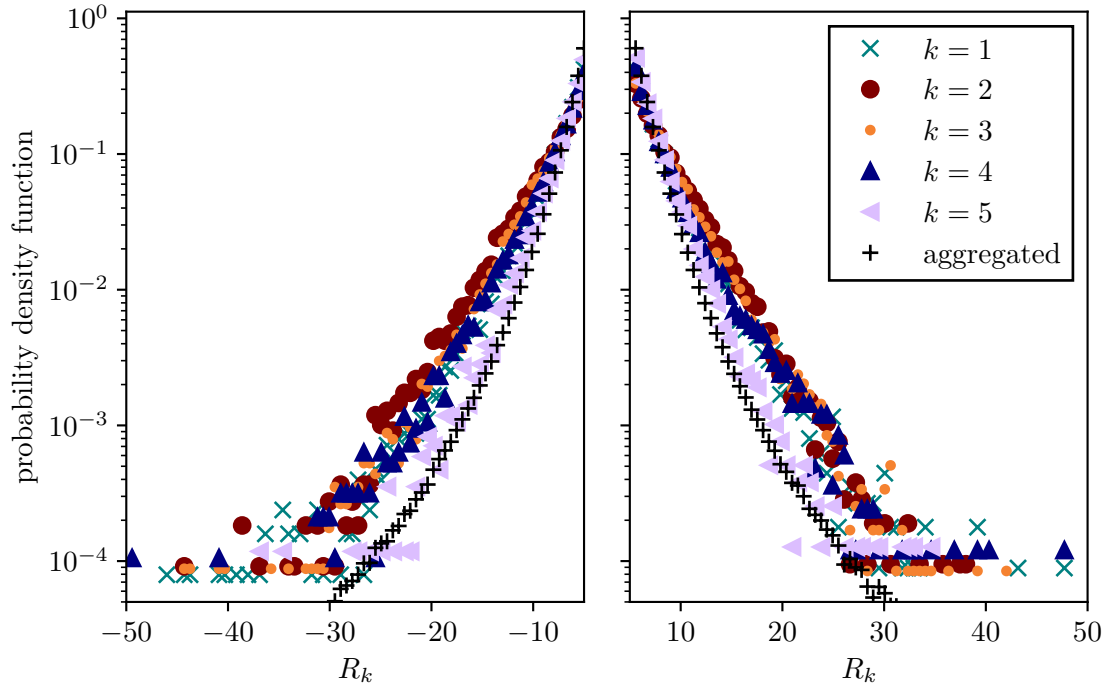


Figure 7: Left and right tails of the probability density functions for the modes (rotated and rescaled) referring to the five largest eigenvalues and the aggregation of all modes.

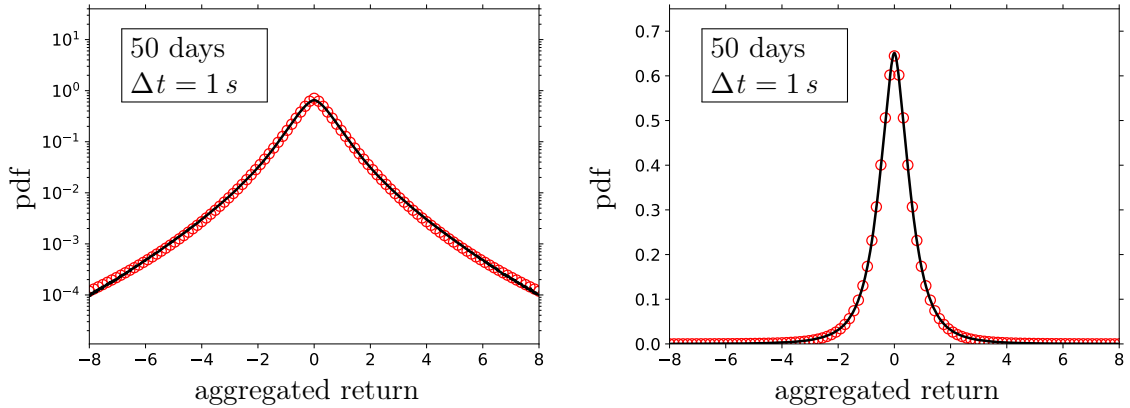


Figure 8: Probability density function for aggregated returns in a time interval of 50 days in 2014, with return horizon 1s. Obtained empirically (black line) and generated by a random matrix model (red circles). Left: Ordinate logarithmically scaled. Right: Ordinate linearly scaled. Adapted from Ref. [14].

holds less weight than the density of the modes. For larger  $|R_k| \gtrsim 20$  a comparison between densities is difficult due to the drastic difference in statistical significance for aggregated and single  $k$ . However, this means that the first few modes referring to the collective market and sectors show greater risk than the average mode referring to an eigenvalue from the bulk and thus a structureless, random linear combination of returns.

We have defined the rotation and rescaling (21) that transforms correlated returns into mutually uncorrelated, variance-normalized modes. In the remainder of the paper, extreme value statistics are applied to these modes rather than to the raw asset returns. In Sec. 5 we analyze these first five modes with regard to their tail behavior.

## 4.2 Connection to Portfolio Risk Management

If we consider a specific mode and therefore fix  $k$ , we have

$$R_k(t) = \Lambda_k^{-1/2} \sum_{l=1}^K U_{lk} M_l(t). \quad (22)$$

This resembles the portfolio return  $W(t)$  in modern portfolio theory, which is usually defined by

$$W(t) = \sum_{l=1}^K g_l(t) Y_l(t), \quad \sum_{l=1}^K g_l(t) = 1, \quad (23)$$

where  $Y_l(t)$  is the return of asset  $l$  at time  $t$  and  $g_l(t)$  is the fractional weight of asset  $l$  in the portfolio. Thus we can view our modes  $R_k(t)$  as similar to  $W(t)$  for distinct choices of portfolios. The entries  $U_{lk}$  of the eigenvectors take the role of the weights  $g_l$  in the case of no turnover. In Fig. 5 we see that all stocks contribute somewhat equally to the first eigenvector corresponding to the largest eigenvalue, which therefore resembles a diversified portfolio choice covering the whole market. Thus our first mode  $R_1(t)$  is similar to the return of such a market-wide portfolio. Since the portfolio is broadly diversified, it is exposed to the pure systematic risk, while idiosyncratic risk is largely diversified away. Contrasting that, the entries in the second eigenvector, corresponding to the second largest eigenvalue, are mostly constituted of stocks from the Energy sector, thus  $R_2(t)$  is similar to the return of an investment portfolio focused on energy. Such a sector-concentrated portfolio is exposed to both systematic risk and substantial idiosyncratic risk, the latter of which can be reduced by broader diversification. In the following we analyze the extremal behavior of the  $R_k(t)$ , and we will see that the tail behavior differs. So this connection highlights the relevance of our approach to portfolio risk management.

## 5 Results

The return modes differ in their tail behavior. As linear combinations of stocks with similar dynamics, they capture correlated behavior. In Sec. 5.1, we apply the POT approach to the marginal data of the modes corresponding to the five largest eigenvalues. This addresses

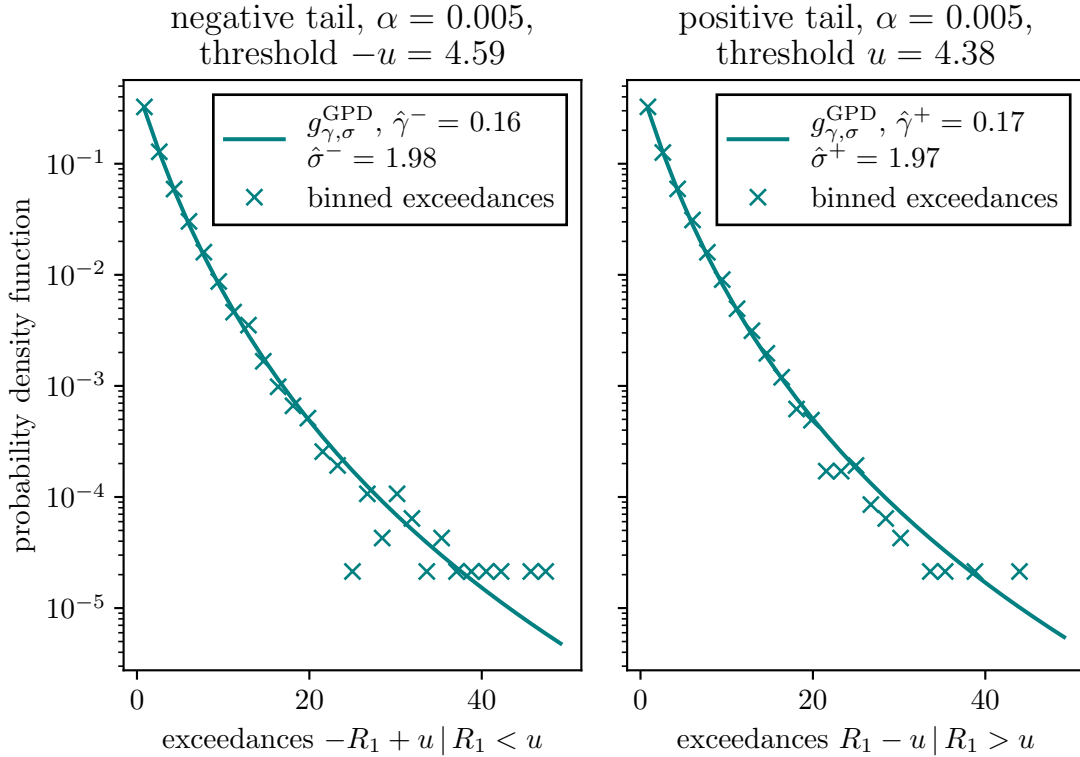


Figure 9: Binned exceedances for both tails of the first mode with tail-quantile  $\alpha = 0.005$  together with the theoretical density function  $g_{\gamma,\sigma}^{\text{GPD}}$  obtained from the fits.

the third point of the paper’s guiding questions. Section 5.2 deals with an estimation for the same modes, but accounting for nonstationarity and seasonality in the form of volatility clustering, referring to the fourth and last point of the paper’s guiding questions.

## 5.1 Estimation for Marginal Distribution

In theory the estimation only using the marginal distribution should suffice, if the dynamics are stationary, the threshold is large enough and the condition **D** is met, as mentioned in Sec. 2. We denote the tail-quantile by  $\alpha$ , implicitly defining the threshold  $u$  for estimation, as sketched in Fig. 4. Results for the tail behaviors  $\hat{\gamma}^+$  (positive tail), and  $\hat{\gamma}^-$  (negative tail) are depicted versus tail-quantile  $\alpha$  and threshold  $u$  in Fig. 10, respective Fig. 11. In addition the NRMSD is shown, to provide an estimate of the goodness-of-fit. To illustrate how the fitted probability densities appear, we depict an example in Fig. 9. In this Fig. 9, we show the empirical density of exceedances together with the corresponding theoretical probability distribution Eq. (7), with fit parameters determined as explained above, for an exemplary tail-quantile and the first mode.

We find that the minimum of the NRMSD coincides with the optimal threshold, which is also visible in a stabilisation of the fitted tail indices  $\hat{\gamma}$ . For both tails and for all modes, the

estimated  $\hat{\gamma}$  differs, but the behavior is mostly of the Fréchet-type. This is expected for high-frequency financial returns which are heavy-tailed, *cf.* Ref. [49]. It is strongly dependent on the threshold  $u$ , similar behavior was already reported in Refs. [49, 50] for individual companies and indices. However, the reported values there refer to returns with much larger return horizons  $\Delta t$ , starting at a scale of minutes. In addition, we see in the NRMSD that the optimal threshold for estimation differs for different modes, and that all modes converge to the GPD with different velocities.

The results for the clustering indices  $\hat{\Theta}^+$  (positive tail) and  $\hat{\Theta}^-$  (negative tail) are shown in Figs. 12 and 13. The estimate of the extremal index  $\hat{\Theta}$  differs from unity in all cases, indicating clustered extremes in all evaluated modes and for both tails. This is consistent with volatility clustering, which is reflected in the clustering of extreme values. The effect is not limited to small tail-quantiles  $\alpha$ , which implies that even at longer time scales there are correlations between extremes. The fact that financial markets show autocorrelations in nonlinear transformations of returns on a long timescale, is well-established [8]. In Fig. 14, the autocorrelation for the absolute values of returns is plotted for the five first modes. We notice that the different levels of persistence in the autocorrelations of the modes are in accordance with the picture from our analysis of the extremal index.

The second mode, corresponding to the Energy sector, shows a significant crossing into the Gumbel or Weibull domain in the positive tail for very high thresholds  $u$ . In addition, it is also the mode with strongest serial clustering and persistence of volatility autocorrelations. These effects are even stronger than the effect on the first mode, *i.e.*, the whole market itself and suggest that the Energy sector exhibits a different extremal behavior than the market and other sectors in the year 2014.

We stress that the strength of our approach lies in reliably estimating  $\gamma$ , but in addition it is even possible to calculate the parameters  $a$  and  $b$  for the corresponding probability density (3) using (6) and by matching the return periods as described in Refs. [27, 51]. We note that the probability densities are then theoretically inferred densities of block maxima, *not* measured block maxima densities. We show the probability densities for the daily maximum in Fig. 15, estimated via the GPD fit at an exemplary threshold of  $u = 15$ . To prove that the calculation of the parameters  $a$  and  $b$  gives indeed the correct result, we show the empirical daily block maxima densities together with our inferred densities in Fig. 16. The distributions fit remarkably well. This is to the best of our knowledge the first empirical analysis of this depth, showing the theoretical correspondence of the POT approach to block maxima methods empirically. It proves that we can avoid the block maxima method entirely, since all information about maxima and minima are contained in the tail of the density. We note that until now, our methods do not treat the nonstationarity of the time series directly. Thus the resulting extreme value statistics should be understood as results of averaging over these effects.

Up to this point we developed the general framework of our analysis and applied it to the rotated modes of financial data. We applied the threshold-based approach to estimate tail behavior and we proved that it allows us to infer also the statistics of the maximum. This checks already three of the four guiding points layed out in the introduction of this paper. We have also begun to address the remaining point — nonstationarity — by demonstrating that seasonalities and extremal clustering are present in our data.

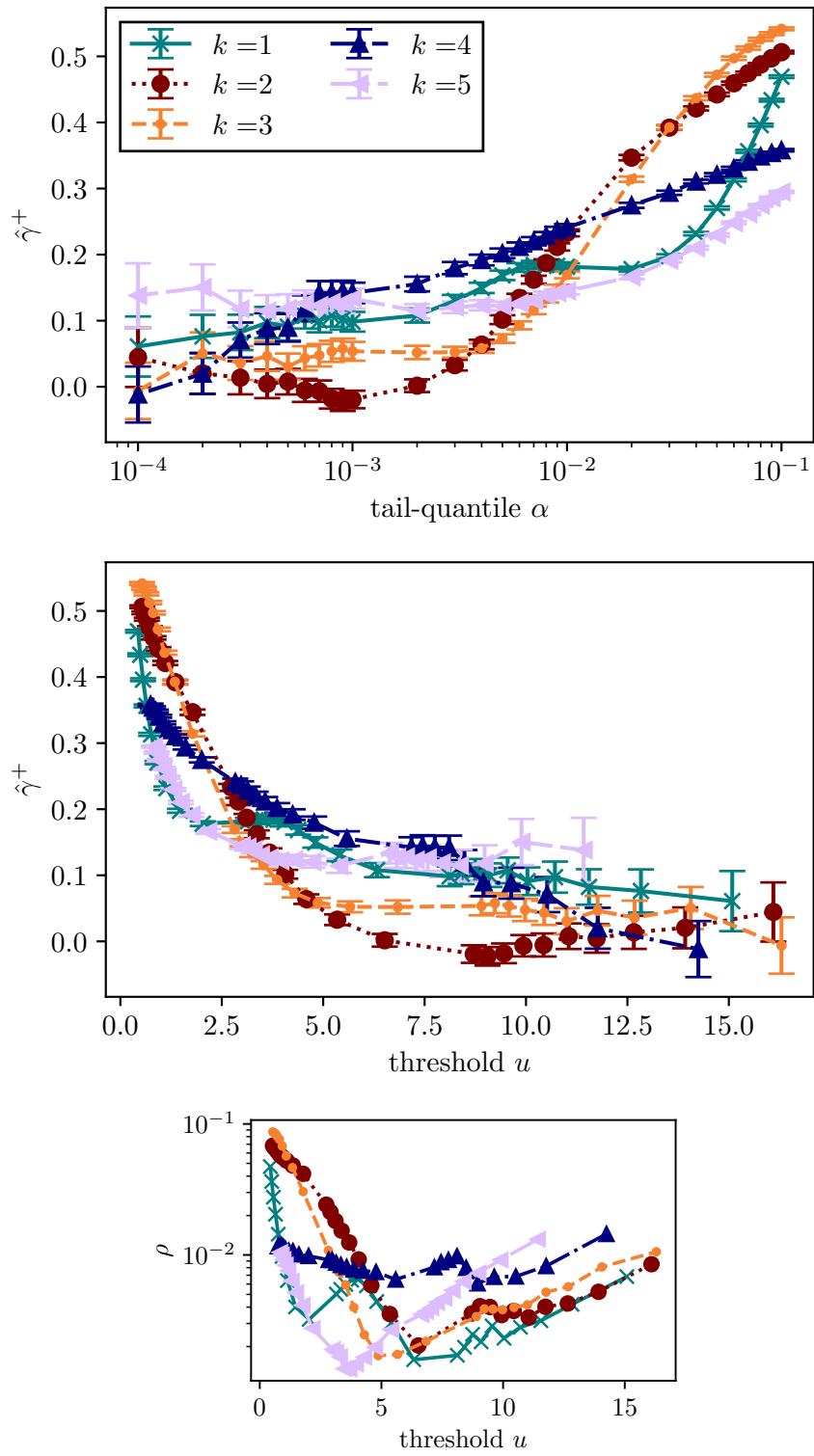


Figure 10: Naive estimation of tail shape parameter without declustering extreme values. Top: Estimated  $\hat{\gamma}^+$  against tail-quantile  $\alpha$ . Middle: Estimated  $\hat{\gamma}^+$  against threshold  $u$ . Standard errors according to (17). Bottom: NRMSD of estimation.

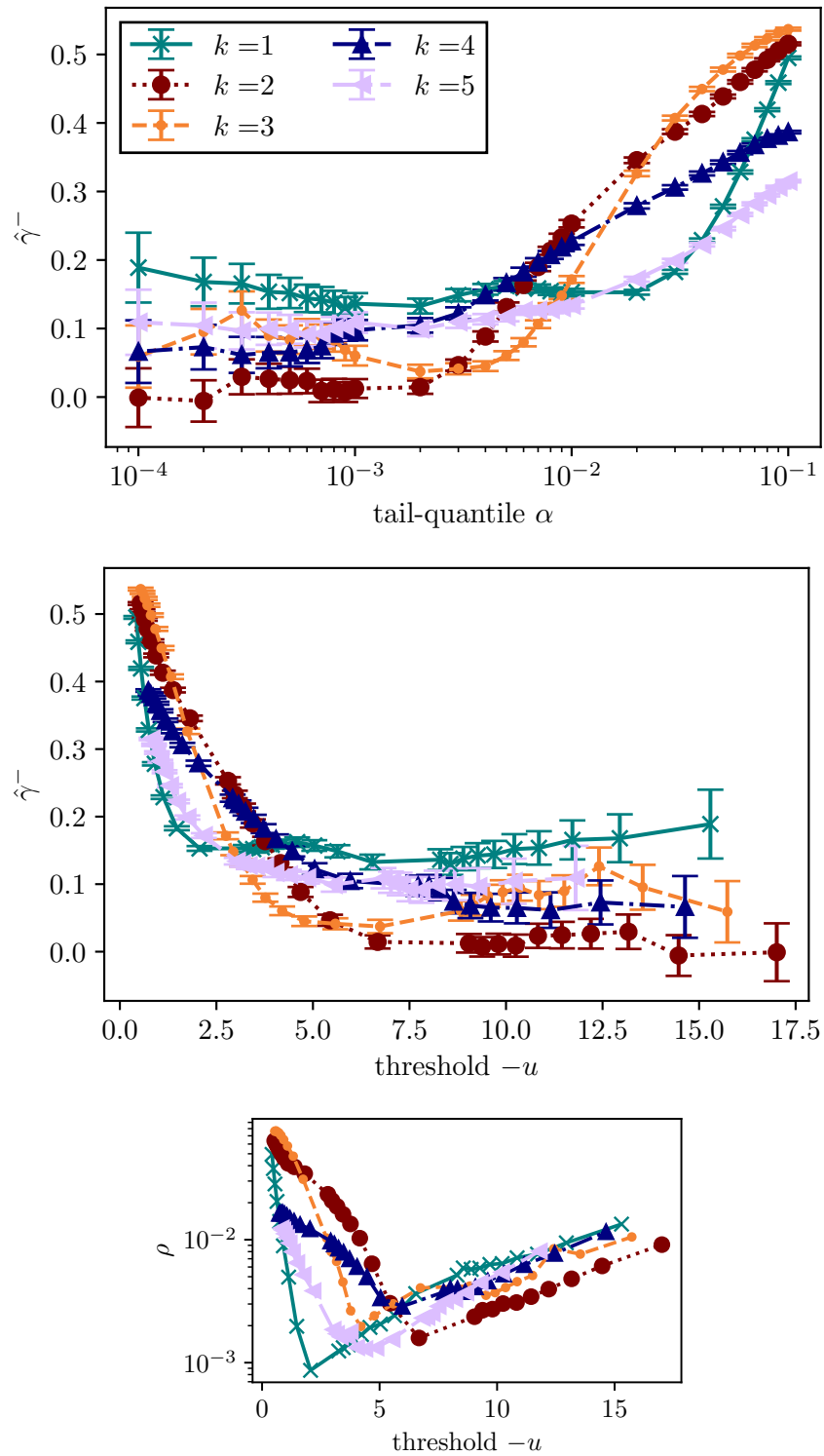


Figure 11: Naive estimation of tail shape parameter without declustering extreme values. Top: Estimated  $\hat{\gamma}^-$  against tail-quantile  $\alpha$ . Middle: Estimated  $\hat{\gamma}^-$  against threshold  $-u$ . Standard errors according to (17). Bottom: NRMSD of estimation.

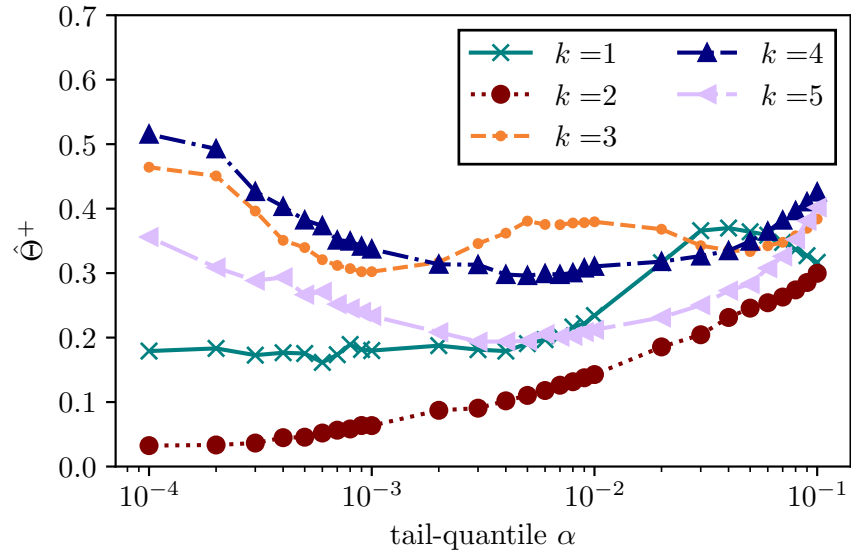


Figure 12: Estimated extremal index  $\hat{\Theta}^+$  against tail-quantile  $\alpha$ .

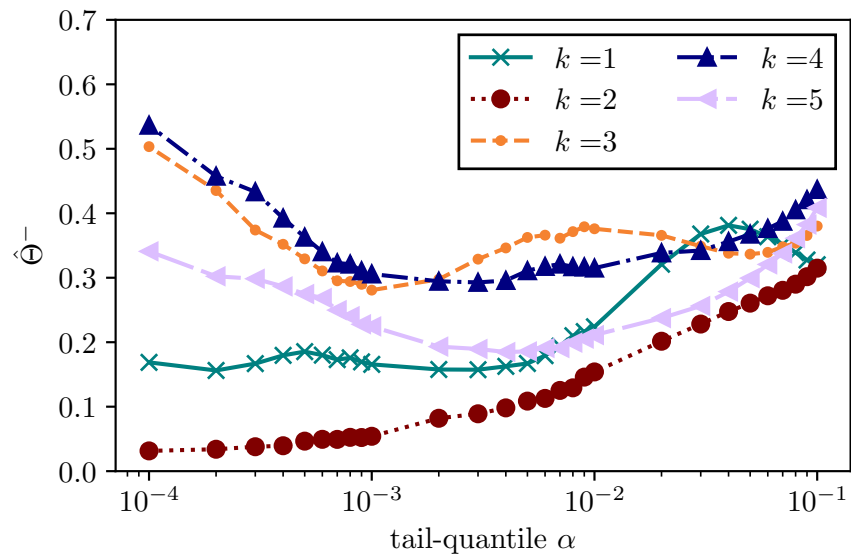


Figure 13: Estimated extremal index  $\hat{\Theta}^-$  against tail-quantile  $\alpha$ .

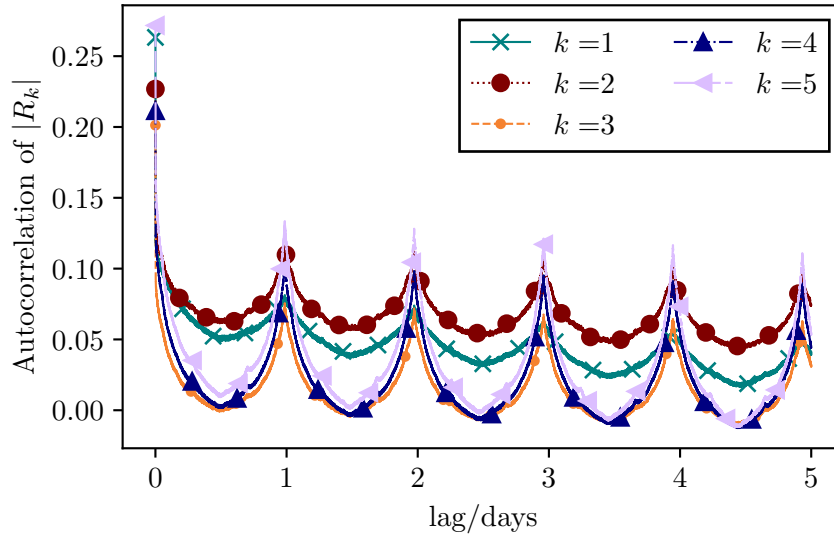


Figure 14: Autocorrelation of absolute values of rotated return modes  $|R_k|$ , against time lag. The first value for each mode is plotted at a lag of 1s. Markers are evenly spaced for better readability, data frequency is 1s.

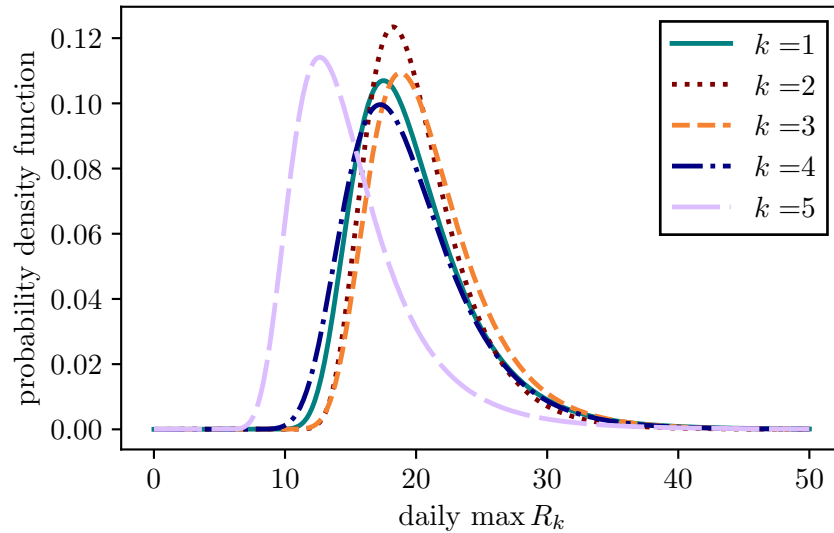


Figure 15: Probability densities  $g_{\gamma,b,a}^{\text{EV}}$  for maxima of the first 5 modes,  $\hat{\gamma}^+, \hat{\sigma}^+$  estimated at a threshold of  $u = 15$  with POT.

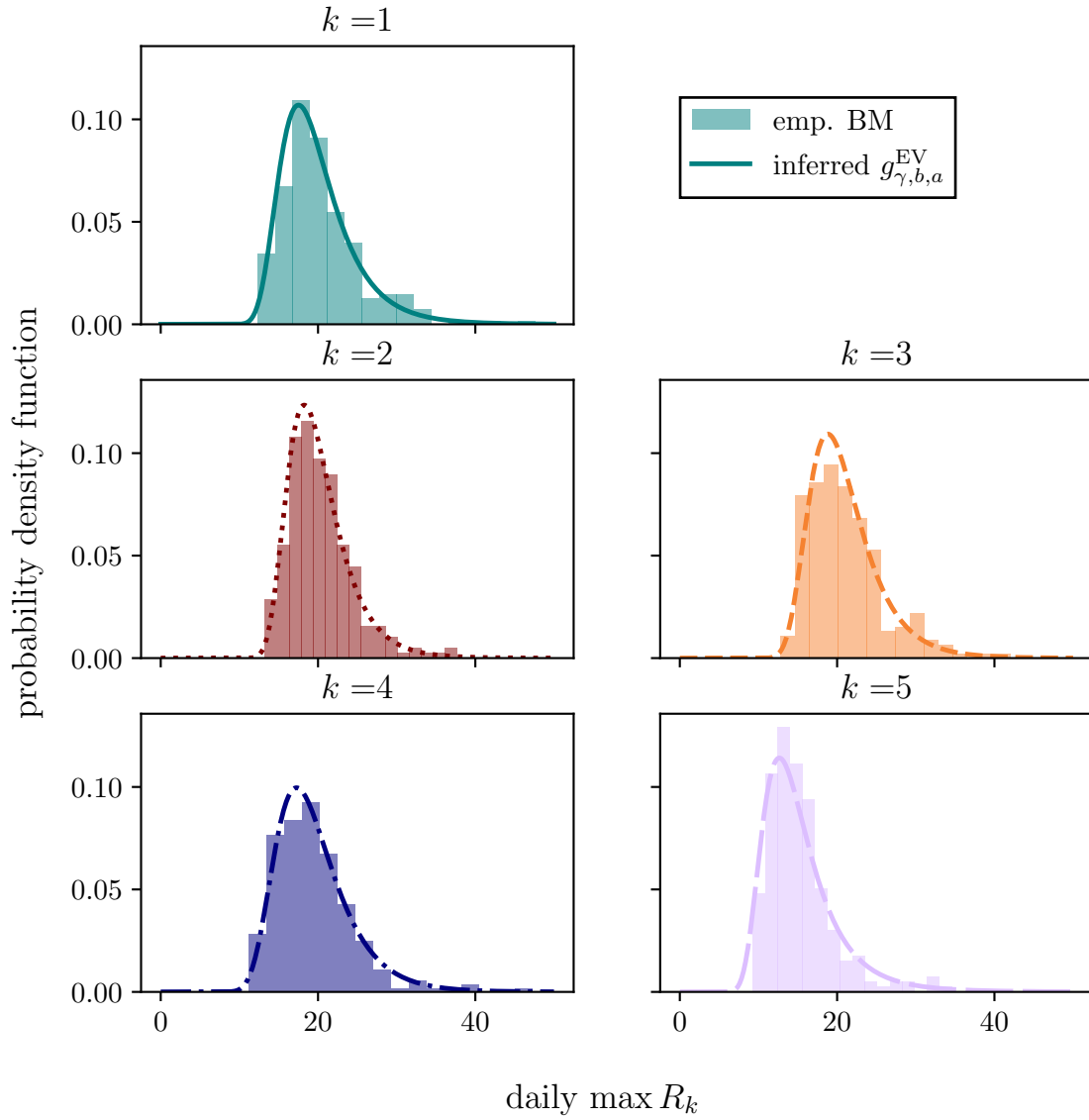


Figure 16: Probability densities  $g_{\gamma, b, a}^{EV}$  for maxima of the first 5 modes,  $\hat{\gamma}^+, \hat{\sigma}^+$  estimated at a threshold of  $u = 15$  with POT in comparison with the empirical probability densities obtained via block maxima.

## 5.2 Residual Risk and Local Threshold Estimation

As shown in Sec. 5.1, there exist strong intraday seasonality effects, in addition to the usual persistence of the volatility autocorrelations. This section addresses point four of our guiding questions, namely how to treat nonstationarity in extreme value analysis at high frequency.

To distinguish between the more deterministic, seasonal risk and the really unpredictable, residual risk, we calculate the mean intraday volatility profile of the modes as [52–54]

$$V_k(t_{\text{intra}}) = \frac{1}{N_{\text{days}}} \sum_{d=0}^{N_{\text{days}}-1} |R_k(d T_{\text{day}} + t_{\text{intra}})|, \quad t_{\text{intra}} = 1, \dots, T_{\text{day}}. \quad (24)$$

Here,  $t_{\text{intra}}$  denotes the intraday time index in seconds. We compute the profile by aligning all trading days and averaging the absolute returns at the same intraday time.

Volatility in the beginning and end of a trading day is generally higher, see for instance Refs. [52, 54–56]. In addition, at a resolution of seconds, spikes occur at distinct times of the day, see Fig. 17. As discussed in Sec. 3.1, spikes would occur also in the end of the trading day, starting at 15:45:00 when information regarding closing auctions is shared with all traders. However, there are similarly sharp spikes throughout the day visible in the volatility profiles for all modes and even for single stocks. Most of these spikes happen at half hour changes, and they are rather stationary throughout the whole year. Due to their sharpness they quickly wash out and are thus not visible in most documented intraday volatility profiles with return horizons of minutes [52, 54, 55]. To the best of our knowledge, there is no documented recurring official information release at these times throughout the day. Therefore it is probable that these seconds of increased volatility emerge due to certain trading or rebalancing algorithms and are thus part of natural trading dynamics. Since these spikes are rather predictable in their occurrence and naturally lead to extreme values in returns, it is of interest to distinguish the natural, residual risk of trading from the systematic, regularly occurring risk, especially in our setting of high frequency. We calculate the residual time series of the modes by dividing the returns of the mode by the intraday volatility profile [52, 54]

$$\tilde{R}_k(t) = R_k(t)/V_k(t \bmod T_{\text{day}}), \quad t = 1, \dots, T. \quad (25)$$

When evaluating the extremal index and the autocorrelation of  $\tilde{R}_k(t)$  we see that the intraday seasonality is removed, and that it is not responsible for the serial clustering of extremes, see Figs. 18 and 19. On the contrary, significant autocorrelation is still apparent and extremes are clustering very strongly.

Thus rather than quantifying the shape parameter of the distribution with a fixed threshold  $u$ , we apply a dynamic threshold  $u(t)$  evaluated by estimating local quantiles with a rolling window. This takes into account the nonstationarity of the return time series, even exogenous effects are incorporated into the rolling window after a few seconds. We have to ensure the window is large enough to contain data points which exceed the local threshold implicitly set by the quantile, since otherwise we will not have any exceedances overall. On the other hand we want to cover the effect of nonstationarity, which limits the length of the window. However, the choice of window size is robust in a range of different lengths, as long

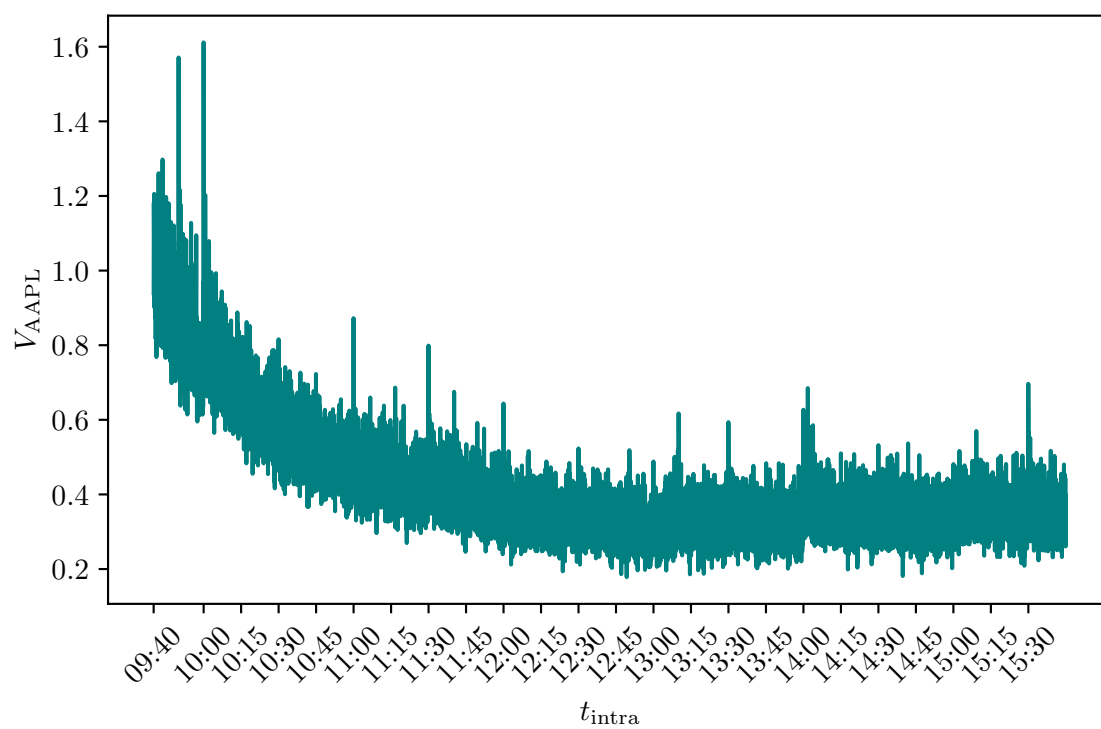
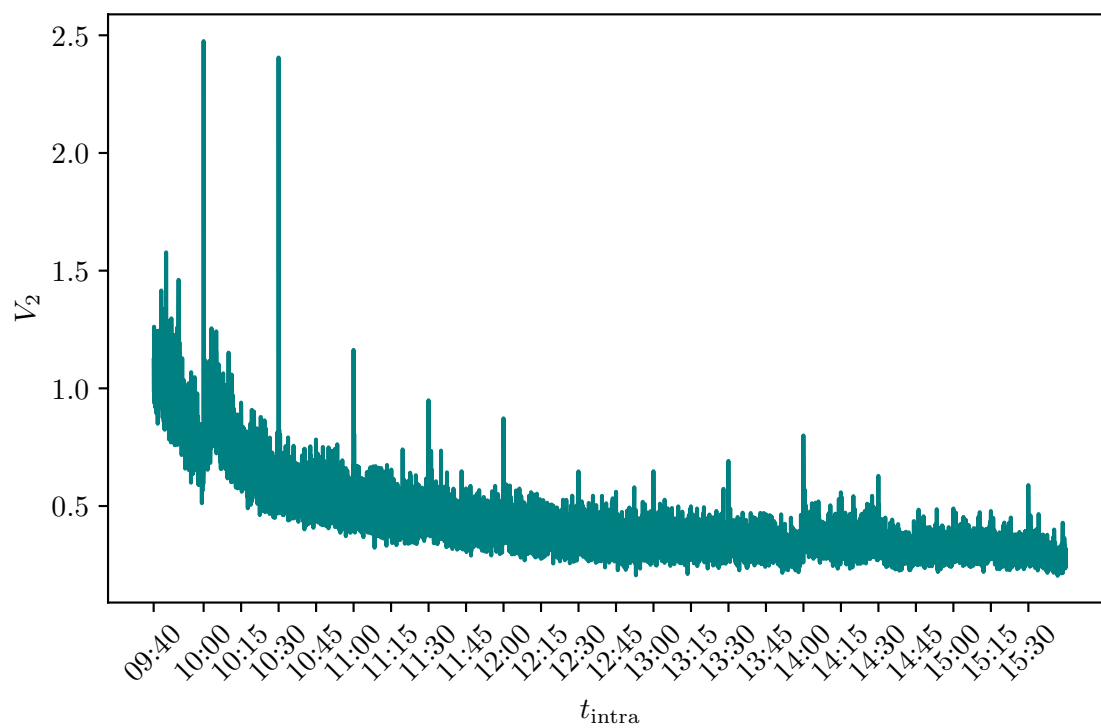


Figure 17: Top: Volatility profile of the second mode  $V_2$  referring to the Energy sector. Bottom: Volatility profile of the stock returns of AAPL  $V_{\text{AAPL}}$ .

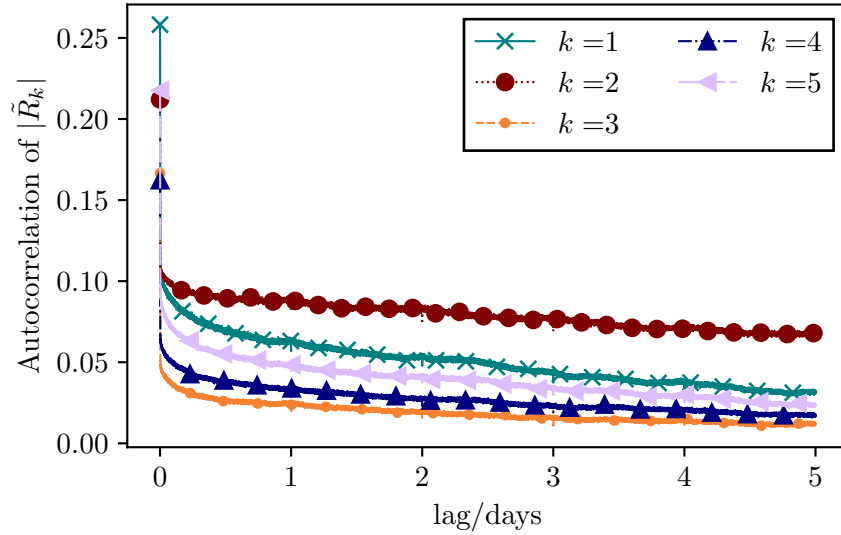


Figure 18: Autocorrelation of absolute values residual time series of rotated return modes  $|\tilde{R}_k|$ , against time lag. The first value for each mode is plotted at a lag of 1s. Markers are evenly spaced for better readability, data frequency is 1s.

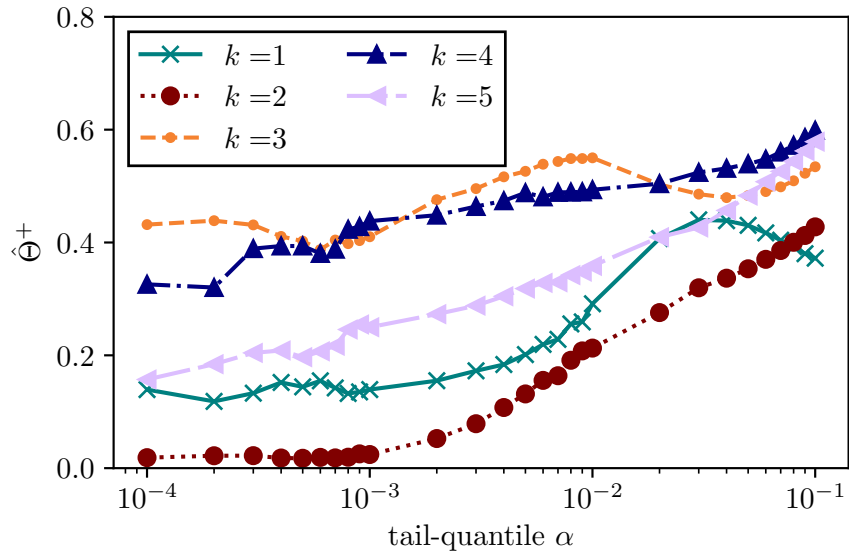


Figure 19: Estimated extremal index  $\hat{\Theta}^+$  of  $\tilde{R}_k$  against tail-quantile  $\alpha$ .

as  $\alpha$  multiplied with the window size is at the scale of one or larger. In that case we have on average one exceedance per window and can reliably estimate the GPD parameters. We find that a window of 10000s, roughly half a trading day, provides a good balance between these aspects. This length allows us to measure extremes up to a quantile of 99.99% while still accounting for nonstationarity. Displaying the local 99.9%-quantile over a rolling window of 10000s in Fig. 20, this nonstationarity is very apparent. Using constant thresholds leads inevitably to clustering of extremes in such cases, as the definition of what is "extreme" changes with the change of the current state of the market.

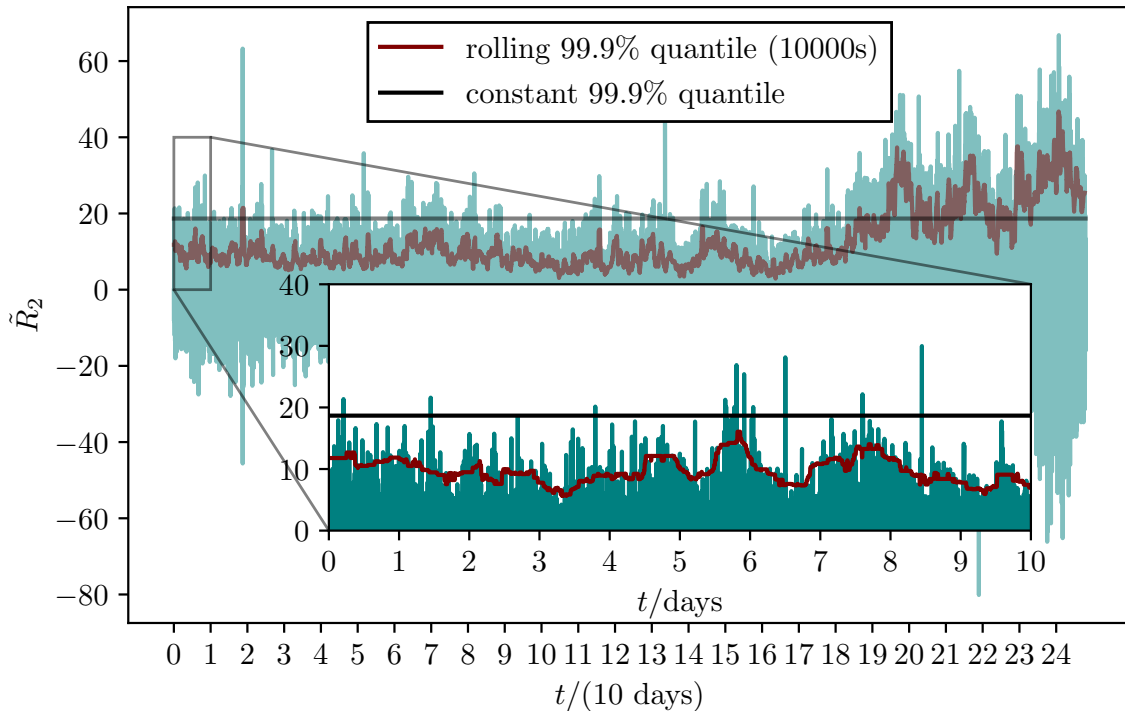


Figure 20: Residuals of mode 2, constant 99.9% quantile and the local rolling 99.9% quantile calculated over the last 10000s.

In Fig. 21, the clustering index is plotted against the tail-quantile  $\alpha$ , which is estimated in a rolling window. Such a local threshold has to remove any serial dependence and autocorrelations by design, and we notice that  $\hat{\Theta}^+$  is considerably higher than for the estimation with nonlocal thresholds. As the threshold tends to tail-quantiles which are high compared to the window size of 10000 data points, the serial dependence is vanishing completely. This is clearly a feature of the rolling window approach, since extremes which lie outside the current window, are not related to extremes inside the current window.

We also notice from the NRMSD in Fig. 21 that the range of the goodness-of-fit is roughly equal to the range of the goodness-of-fit for the estimation method using fixed  $u$ . The distributions obtained with our local threshold method applied to the residuals of the modes converge to a generalized Pareto distribution, justifying our approach mathematically.

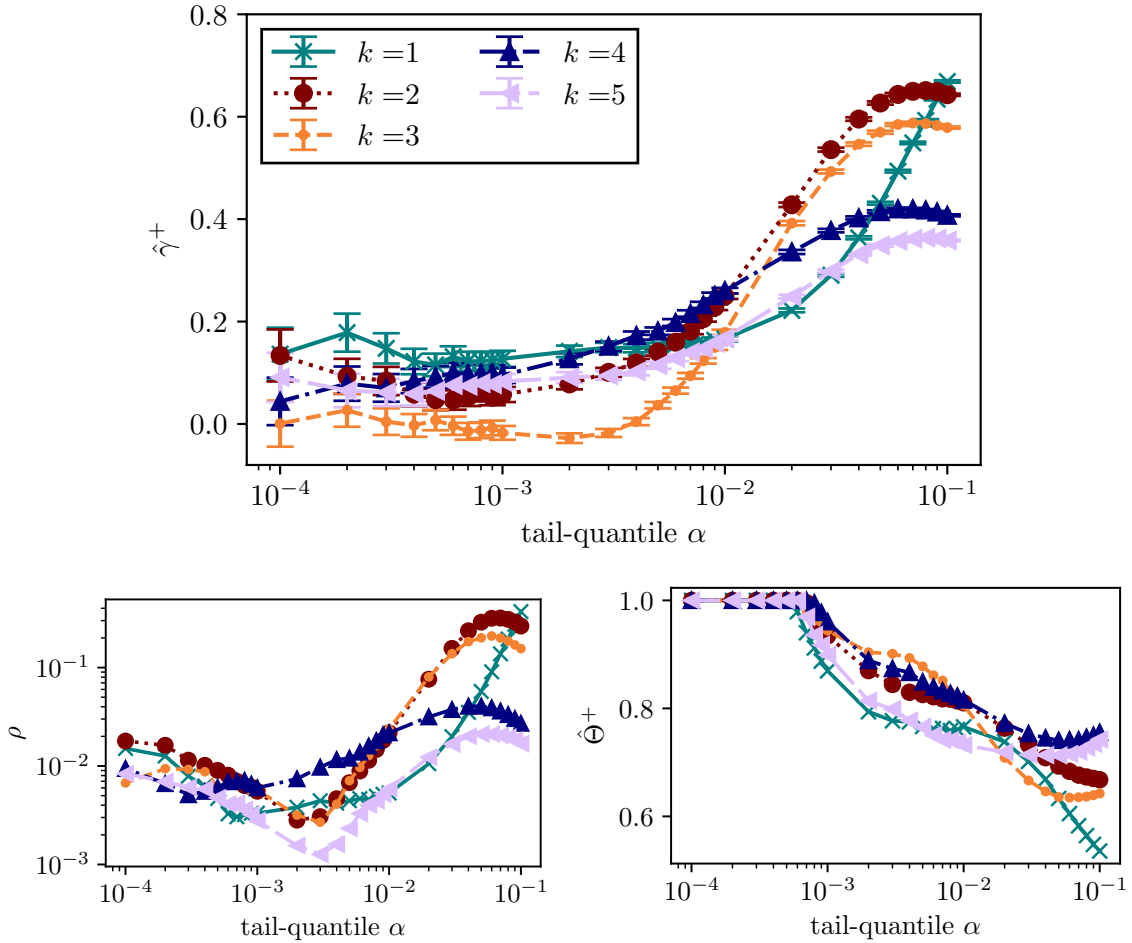


Figure 21: Estimation of positive tail shape parameter  $\hat{\gamma}^+$  with a rolling threshold determined by the local tail-quantile  $\alpha$  over 10000s. Top: Estimated  $\hat{\gamma}$ , standard errors according to (17). Bottom left: NRMSD of estimation. Bottom right: Estimated extremal index  $\hat{\Theta}^+$ .

Our results using a local threshold and the deseasonalized residuals of the modes differ quantitatively from the results of the method using fixed  $u$ . Although the range of the tail index is roughly the same, we see that the ordering of the modes indeed changes. Not all modes are influenced with the same strength by the effects of nonstationarity and intraday volatility clustering, thus leading to these changes in order.

As in Sec. 5.1, it is possible to calculate the parameters  $a$  and  $b$  of (3). Since we use a dynamic threshold  $u(t)$  here our location parameter  $b(t)$  is time dependent. We show the nonstationary probability density  $g_{\gamma, b(t), a}^{\text{EV}}$  for the positive extremes of the second mode as an example in a time range of forty days in Fig. 22. What we see is that the density of observing a daily extreme, given the current local threshold  $u(t)$ , changes location drastically in time.

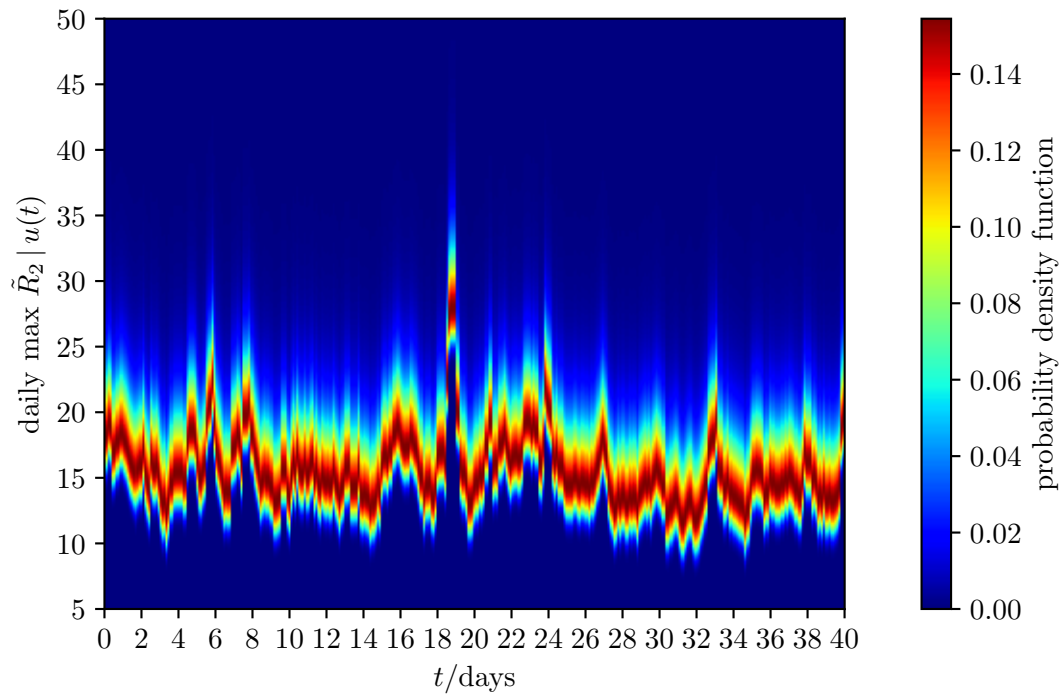


Figure 22: Nonstationary probability density  $g_{\gamma, b(t), a}^{\text{EV}}$  of the second mode plotted for forty consecutive trading days. Estimated via local rolling 99.9% quantile calculated over the last 10000s. Time resolution is 1s, the probability density function is normalized in each time step  $t$ .

### 5.3 Interpretation

When interpreting the results obtained in Secs. 5.1 and 5.2, it is crucial to distinguish the different scenarios. In both scenarios we analyzed the return modes, *i.e.*, the return time series of the linear combinations referring to the market and the sectors. These capture the most important dynamics in the large multivariate financial system.

In Sec. 5.1, we analyzed the purely marginal distributions of the modes in one year. This allows us to make statements about the risk profile of the market and its sectors on an annual basis. The quantified risk here includes the rather deterministic surges of volatility and the seasonality effects we showed in Sec. 5.2 and does not take into account a nonstationary notion of risk aversion. The threshold of what counts as "extreme" in this estimation is set in hindsight and remains fixed, even when the markets themselves become more volatile.

In Sec. 5.2, the perspective is different. Here, we quantify the underlying residual risk while explicitly accounting for the known seasonality profile and the changing risk profile in the state of the market itself. When trading at high frequencies, risk can only be evaluated according to the current market state. For trading strategies that aim at small profits on timescales of seconds, it is not sensible to evaluate risks relative to an annual benchmark. Risk factors of seasonality and known recurring volatility bursts are accounted for beforehand. A sharp peak in volatility for instance is not unusual but expected in the morning of a trading day, and is thus much less an "extreme" event than the same peak during midday. So we take the actual residual risk and evaluate it in comparison to the benchmark of the market risk, which is measured locally through a rolling quantile estimation. We see that local thresholds make the notion of an "extreme" adaptive to the current market state and substantially reduce spurious clustering induced by regime shifts. This addresses the fourth — and final — guiding point of this paper.

We proved that our general approach works well and that it can be adapted to different scenarios.

## 6 Conclusion

Quantifying risk in complex systems — exemplary in financial markets where dependencies exist across time, across system constituents, and under nonstationary conditions — is crucial for understanding and anticipating systemic vulnerabilities. It is also essential for the evaluation of extreme event likelihoods and the design of robust strategies for risk management.

We addressed four guiding points laid out in the introduction. *First*, we developed a general framework for extreme-value analysis in multivariate, strongly correlated time series by reducing the problem to a set of interpretable collective coordinates. *Second*, we rotated high-frequency stock returns into the eigenbasis of the correlation matrix, yielding modes that can be interpreted as collective dynamics of the market and sectoral activity. *Third*, we used the POT approach based on a GPD fit to uncover tail behaviour and, via the correspondence between the GPD and the extreme value distribution, to infer the implied statistics of block maxima without relying on a block maxima estimation procedure. In contrast to the block maxima method, the POT approach is more efficient in data usage and

it does not rely on a fixed compartmentalization in the time domain. *Fourth*, we explicitly accounted for nonstationarity by removing intraday seasonality through volatility profiling and by employing local, time dependent thresholds estimated from rolling quantiles to obtain a market state dependent notion of extremes.

To the best of our knowledge, this is the first systematic application of extreme value theory to return modes with frequencies on the scale of seconds obtained from an eigenbasis decomposition, which allows disentangling collective and sectoral sources of risk.

Our results for financial data extend and are consistent with other analyses of tail behavior, usually done for higher return horizons and for indices and single stocks. We show that the extreme value distributions of the market and the sectors lie qualitatively in the Fréchet domain, at high frequency horizons of seconds. Quantitatively, the tail shape parameters differ. Strengths of serial dependencies also differ strongly between modes, with the market and the Energy sector displaying the highest amount of clustering for extreme events. We analyzed the residuals of the return modes, by weighting the time series according to their average intraday volatility profile. This allowed us to focus on the pure stochastic risk. Our analysis proved that the serial dependence is not due to the intraday seasonalities and intraday volatility clustering, but rather due to dependencies on longer time scales and nonstationarities in the volatility. Using local thresholds, we estimate extremal behavior conditional on the current market state. From this local perspective, the tails remain of Fréchet type, but the relative susceptibility of modes to extremes changes due to differing levels of dependence and nonstationarity.

Since our approach is general and not limited to linear measures such as the Pearson correlation used in our example study, the analysis can be extended to include measures focusing directly on extreme values such as matrices of pairwise tail dependencies *et cetera*. Nonlinear measures may be able to order stocks according to their similarity regarding only their extremal behavior. Importantly the method is not limited to financial data and there is a plethora of multivariate systems where such an analysis can provide value in understanding the dynamics and statistics of collective extremal behavior.

## References

- [1] P. Sura, “A General Perspective of Extreme Events in Weather and Climate”, *Atmospheric Research* **101**, 1 (2011).
- [2] L. Cheng, A. AghaKouchak, E. Gilleland, and R. W. Katz, “Non-Stationary Extreme Value Analysis in a Changing Climate”, *Climatic Change* **127**, 353 (2014).
- [3] K. Engeland, H. Hisdal, and A. Frigessi, “Practical Extreme Value Modelling of Hydrological Floods and Droughts: A Case Study”, *Extremes* **7**, 5 (2004).
- [4] P. Songchitruksa and A. P. Tarko, “The Extreme Value Theory Approach to Safety Estimation”, *Accident Analysis & Prevention* **38**, 811 (2006).
- [5] K. G. Koedijk, M. M. A. Schafgans, and C. G. de Vries, “The Tail Index of Exchange Rate Returns”, *Journal of International Economics* **29**, 93 (1990).
- [6] P. Embrechts, C. Klüppelberg, and T. Mikosch, *Modelling Extremal Events* (Springer Berlin Heidelberg, Berlin, Heidelberg, 1997).
- [7] H. Markowitz, “Portfolio Selection”, *The Journal of Finance* **7**, 77 (1952).
- [8] Z. Ding, C. W. J. Granger, and R. F. Engle, “A Long Memory Property of Stock Market Returns and a New Model”, *Journal of Empirical Finance* **1**, 83 (1993).
- [9] T. Lux, “Long-Term Stochastic Dependence in Financial Prices: Evidence from the German Stock Market”, *Applied Economics Letters* **3**, 701 (1996).
- [10] M. C. Münnix and R. Schäfer, “A Copula Approach on the Dynamics of Statistical Dependencies in the US Stock Market”, *Physica A: Statistical Mechanics and its Applications* **390**, 4251 (2011).
- [11] M. C. Münnix, T. Shimada, R. Schäfer, F. Leyvraz, T. H. Seligman, T. Guhr, and H. E. Stanley, “Identifying States of a Financial Market”, *Scientific Reports* **2**, 644 (2012).
- [12] T. Guhr and A. Schell, “Exact multivariate amplitude distributions for non-stationary Gaussian or algebraic fluctuations of covariances or correlations”, *Journal of Physics A: Mathematical and Theoretical* **54**, 125002 (2021).
- [13] E. Manolakis, A. J. Heckens, B. Köhler, and T. Guhr, “Multivariate distributions in non-stationary complex systems I: A random matrix model and formulae for data analysis”, *Journal of Statistical Mechanics: Theory and Experiment* **2025**, 103404 (2025).
- [14] A. J. Heckens, E. Manolakis, C. Schuhmann, and T. Guhr, “Multivariate distributions in non-stationary complex systems II: Empirical results for correlated stock markets”, *Journal of Statistical Mechanics: Theory and Experiment* **2025**, 103405 (2025).
- [15] F. Salmon, “The Formula that Killed Wall Street”, *Significance* **9**, 16 (2012).
- [16] G. Livan, J.-i. Inoue, and E. Scalas, “On the non-stationarity of financial time series: impact on optimal portfolio selection”, *Journal of Statistical Mechanics: Theory and Experiment* **2012**, P07025 (2012).
- [17] R. A. Fisher and L. H. C. Tippett, “Limiting Forms of the Frequency Distribution of the Largest or Smallest Member of a Sample”, *Mathematical Proceedings of the Cambridge Philosophical Society* **24**, 180 (1928).

- [18] B. Gnedenko, “Sur La Distribution Limite Du Terme Maximum D’Une Série Aléatoire”, *Annals of Mathematics* **44**, 423 (1943).
- [19] A. A. Balkema and L. de Haan, “Residual Life Time at Great Age”, *The Annals of Probability* **2**, 792 (1974).
- [20] J. Pickands III, “Statistical Inference Using Extreme Order Statistics”, *The Annals of Statistics* **3**, 119 (1975).
- [21] E. J. Gumbel, “The Return Period of Flood Flows”, *The Annals of Mathematical Statistics* **12**, 163 (1941).
- [22] E. J. Gumbel, “On the Frequency Distribution of Extreme Values in Meteorological Data”, *Bulletin of the American Meteorological Society* **23**, 95 (1942).
- [23] W. Weibull, *A Statistical Theory of the Strength of Materials* (Generalstabens litografiska anstalts förlag, 1939).
- [24] S. N. Majumdar and G. Schehr, *Statistics of Extremes and Records in Random Sequences* (Oxford University Press, July 2024).
- [25] S. N. Majumdar, A. Pal, and G. Schehr, “Extreme value statistics of correlated random variables: A pedagogical review”, *Physics Reports, Extreme Value Statistics of Correlated Random Variables: A Pedagogical Review* **840**, 1 (2020).
- [26] L. Haan and A. Ferreira, *Extreme Value Theory: An Introduction*, Vol. 3 (Springer, 2006).
- [27] S. Coles, *An Introduction to Statistical Modeling of Extreme Values*, Springer Series in Statistics (Springer London, London, 2001).
- [28] F. M. Longin, “The Asymptotic Distribution of Extreme Stock Market Returns”, *The Journal of Business* **69**, 383 (1996).
- [29] J. R. M. Hosking and J. R. Wallis, “Parameter and Quantile Estimation for the Generalized Pareto Distribution”, *Technometrics* **29**, 339 (1987).
- [30] A. J. McNeil and R. Frey, “Estimation of tail-related risk measures for heteroscedastic financial time series: an extreme value approach”, *Journal of Empirical Finance* **7**, 271 (2000).
- [31] M. R. Leadbetter, “On Extreme Values in Stationary Sequences”, *Zeitschrift für Wahrscheinlichkeitstheorie und Verwandte Gebiete* **28**, 289 (1974).
- [32] “Discussion of the Paper by Davison and Smith”, *Journal of the Royal Statistical Society Series B: Statistical Methodology* **52**, 425 (1990).
- [33] A. C. Davison and R. L. Smith, “Models for Exceedances Over High Thresholds”, *Journal of the Royal Statistical Society Series B: Statistical Methodology* **52**, 393 (1990).
- [34] M. R. Leadbetter, “Extremes and Local Dependence in Stationary Sequences”, *Zeitschrift für Wahrscheinlichkeitstheorie und verwandte Gebiete* **65**, 291 (1983).
- [35] N. R. Moloney, D. Faranda, and Y. Sato, “An Overview of the Extremal Index”, *Chaos: An Interdisciplinary Journal of Nonlinear Science* **29**, 022101 (2019).

- [36] C. A. T. Ferro and J. Segers, “Inference for Clusters of Extreme Values”, *Journal of the Royal Statistical Society Series B: Statistical Methodology* **65**, 545 (2003).
- [37] J. Bacidore, B. Polidore, W. Xu, and C. Y. Yang, “Trading around the Close”, *The Journal of Trading* **8**, 48 (2012).
- [38] *NYSE Regulation: Rule Interpretations*, <https://www.nyse.com/regulation/rule-interpretations> (visited on 09/10/2025).
- [39] R. L. Smith, “Threshold Methods for Sample Extremes”, in *Statistical Extremes and Applications*, edited by J. T. de Oliveira (Springer Netherlands, Dordrecht, 1984), pp. 621–638.
- [40] L. Laloux, P. Cizeau, J.-P. Bouchaud, and M. Potters, “Noise Dressing of Financial Correlation Matrices”, *Physical Review Letters* **83**, 1467 (1999).
- [41] MSCI, S&P Dow Jones Indices LLC and its affiliates, “Global Industry Classification Sector (GICS)”, (2023).
- [42] V. Plerou, P. Gopikrishnan, B. Rosenow, L. A. N. Amaral, and H. E. Stanley, “A Random Matrix Theory Approach to Financial Cross-Correlations”, *Physica A: Statistical Mechanics and its Applications* **287**, 374 (2000).
- [43] A. Kessy, A. Lewin, and K. Strimmer, “Optimal Whitening and Decorrelation”, *The American Statistician* **72**, 309 (2018).
- [44] E. T. Phillips and H. Kantz, “Improved Trend Analysis With EOFs and Application to Warming of Polar Regions”, *International Journal of Climatology* **45**, e8823 (2025).
- [45] T. W. Epps, “Comovements in Stock Prices in the Very Short Run”, *Journal of the American Statistical Association* **74**, 291 (1979).
- [46] T. Hayashi and N. Yoshida, “On covariance estimation of non-synchronously observed diffusion processes”, *Bernoulli* **11**, 359 (2005).
- [47] M. C. Münnix, R. Schäfer, and T. Guhr, “Compensating asynchrony effects in the calculation of financial correlations”, *Physica A: Statistical Mechanics and its Applications* **389**, 767 (2010).
- [48] M. C. Münnix, R. Schäfer, and T. Guhr, “Impact of the tick-size on financial returns and correlations”, *Physica A: Statistical Mechanics and its Applications* **389**, 4828 (2010).
- [49] V. Plerou, P. Gopikrishnan, L. A. Nunes Amaral, M. Meyer, and H. E. Stanley, “Scaling of the distribution of price fluctuations of individual companies”, *Physical Review E* **60**, 6519 (1999).
- [50] P. Gopikrishnan, V. Plerou, L. A. Nunes Amaral, M. Meyer, and H. E. Stanley, “Scaling of the distribution of fluctuations of financial market indices”, *Physical Review E* **60**, 5305 (1999).
- [51] Y. Ding, B. Cheng, and Z. Jiang, “A newly-discovered GPD-GEV relationship together with comparing their models of extreme precipitation in summer”, *Advances in Atmospheric Sciences* **25**, 507 (2008).

- [52] Y. Liu, P. Gopikrishnan, Cizeau, Meyer, Peng, and H. E. Stanley, “Statistical properties of the volatility of price fluctuations”, *Physical Review E* **60**, 1390 (1999).
- [53] V. Plerou, P. Gopikrishnan, and H. E. Stanley, “Quantifying fluctuations in market liquidity: Analysis of the bid-ask spread”, *Physical Review E* **71**, 046131 (2005).
- [54] F. Wang, K. Yamasaki, S. Havlin, and H. E. Stanley, “Scaling and memory of intraday volatility return intervals in stock markets”, *Physical Review E* **73**, 026117 (2006).
- [55] L. Harris, “A transaction data study of weekly and intradaily patterns in stock returns”, *Journal of Financial Economics* **16**, 99 (1986).
- [56] A. R. Admati and P. Pfleiderer, “A Theory of Intraday Patterns: Volume and Price Variability”, *The Review of Financial Studies* **1**, 3 (1988).

## A Appendix

### A.1 List of Tickersymbols (alphabetically sorted)

A, AA, AAPL, ABBV, ABC, ABT, ACE, ACN, ACT, ADBE, ADI, ADM, ADP, ADS, ADSK, ADT, AEE, AEP, AES, AET, AFL, AGN, AIG, AIV, AIZ, AKAM, ALL, ALLE, ALTR, ALXN, AMAT, AME, AMGN, AMP, AMT, AMZN, AN, AON, APA, APC, APD, APH, ARG, ATI, AVB, AVP, AVY, AXP, AZO, BA, BAC, BAX, BBBY, BBT, BBY, BCR, BDX, BEN, BHI, BIIB, BK, BLK, BLL, BMY, BRCM, BSX, BWA, BXP, C, CA, CAG, CAH, CAM, CAT, CB, CBG, CBS, CCE, CCI, CCL, CELG, CERN, CF, CFN, CHK, CHRW, CI, CINF, CL, CLX, CMA, CMCSA, CME, CMG, CMI, CMS, CNP, CNX, COF, COG, COH, COL, COP, COST, COV, CPB, CRM, CSC, CSCO, CSX, CTAS, CTL, CTSH, CTXS, CVC, CVS, CVX, D, DAL, DD, DE, DFS, DG, DGX, DHI, DHR, DIS, DISCA, DLPH, DLTR, DNB, DNR, DO, DOV, DOW, DPS, DRI, DTE, DTV, DUK, DVA, DVN, EA, EBAY, ECL, ED, EFX, EIX, EL, EMC, EMN, EMR, EOG, EQR, EQT, ESRX, ESV, ETFC, ETN, ETR, EW, EXC, EXPD, EXPE, F, FAST, FB, FCX, FDO, FDX, FE, FFIV, FIS, FISV, FITB, FLIR, FLR, FLS, FMC, FOSL, FOXA, FSLR, FTI, FTR, GAS, GCI, GD, GE, GGP, GILD, GIS, GLW, GM, GME, GNW, GOOG, GPC, GPS, GRMN, GS, GT, GWW, HAL, HAR, HAS, HBAN, HCBK, HCN, HCP, HD, HES, HIG, HOG, HON, HOT, HP, HPQ, HRB, HRL, HRS, HSP, HST, HSY, HUM, IBM, ICE, IFF, INTC, INTU, IP, IPG, IR, IRM, ISRG, ITW, IVZ, JCI, JEC, JNJ, JNPR, JOY, JPM, JWN, K, KEY, KIM, KLAC, KMB, KMI, KMX, KO, KR, KRFT, KSS, KSU, L, LB, LEG, LEN, LH, LIFE, LLL, LLTC, LLY, LM, LMT, LNC, LO, LOW, LRCX, LUK, LUV, LYB, M, MA, MAC, MAR, MAS, MAT, MCD, MCHP, MCK, MCO, MDLZ, MDT, MET, MHFI, MHK, MJN, MKC, MMC, MMM, MNST, MO, MON, MOS, MPC, MRK, MRO, MS, MSFT, MSI, MTB, MU, MUR, MWV, MYL, NBR, NDAQ, NE, NEE, NEM, NFLX, NFX, NI, NKE, NLSN, NOC, NOV, NRG, NSC, NTAP, NTRS, NUE, NVDA, NWL, NWSA, OI, OKE, OMC, ORCL, ORLY, OXY, PAYX, PBCT, PBI, PCAR, PCG, PCL, PCLN, PCP, PDCO, PEG, PEP, PETM, PFE, PFG, PG, PGR, PH, PHM, PKI, PLD, PLL, PM, PNC, PNR, PNW, POM, PPG, PPL, PRGO, PRU, PSA, PSX, PVH, PWR, PX, PXD, QCOM, QEP, R, RAI, RDC, REGN, RF, RHI, RHT, RIG, RL, ROK, ROP, ROST, RRC, RSG, RTN, SBUX, SCG, SCHW, SE, SEE, SHW, SIAL, SJM, SLB, SNA, SNDK, SNI, SO, SPG, SPLS, SRCL, SRE, STI, STJ, STT, STX, STZ, SWK, SWN, SWY, SYK, SYMC, SYU, T, TAP, TDC, TE, TEG, TEL, TGT, THC, TIF, TJX, TMK, TMO, TRIP, TROW, TRV, TSN, TSO, TSS, TWC, TWX, TXN, TXT, TYC, UNH, UNM, UNP, UPS, URBN, USB, UTX, V, VAR, VFC, VIAB, VLO, VMC, VNO, VRSN, VRTX, VTR, VZ, WAG, WAT, WDC, WEC, WFC, WFM, WHR, WIN, WM, WMB, WMT, WU, WY, WYN, WYNN, XEL, XL, XLNX, XOM, XRAY, XRX, XYL, YHOO, YUM

### A.2 Collection of Q-Q plots

#### A.2.1 Marginal Fit

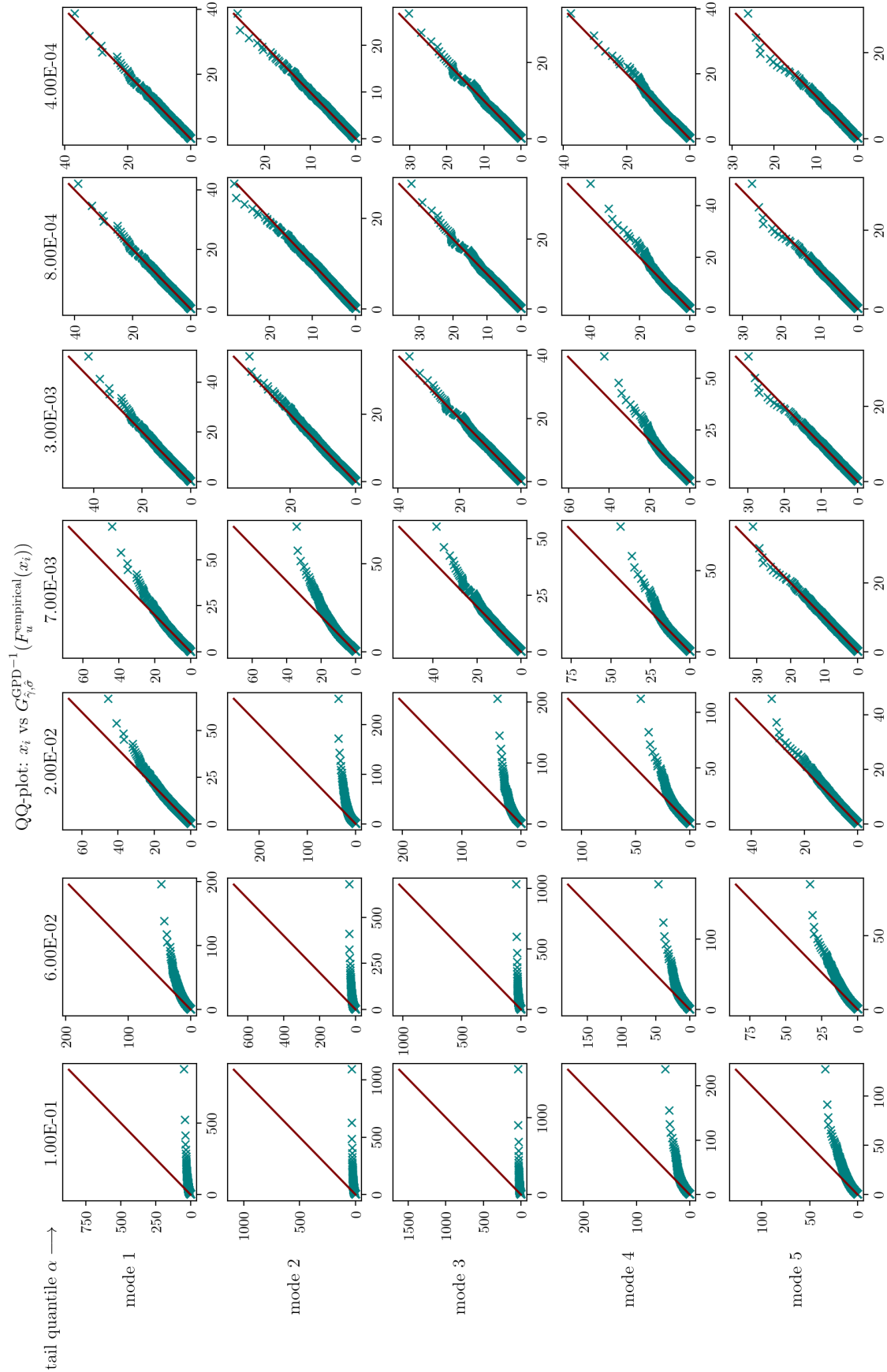


Figure 23: Q-Q plots of fitted GPD with increasing threshold, positive tail.

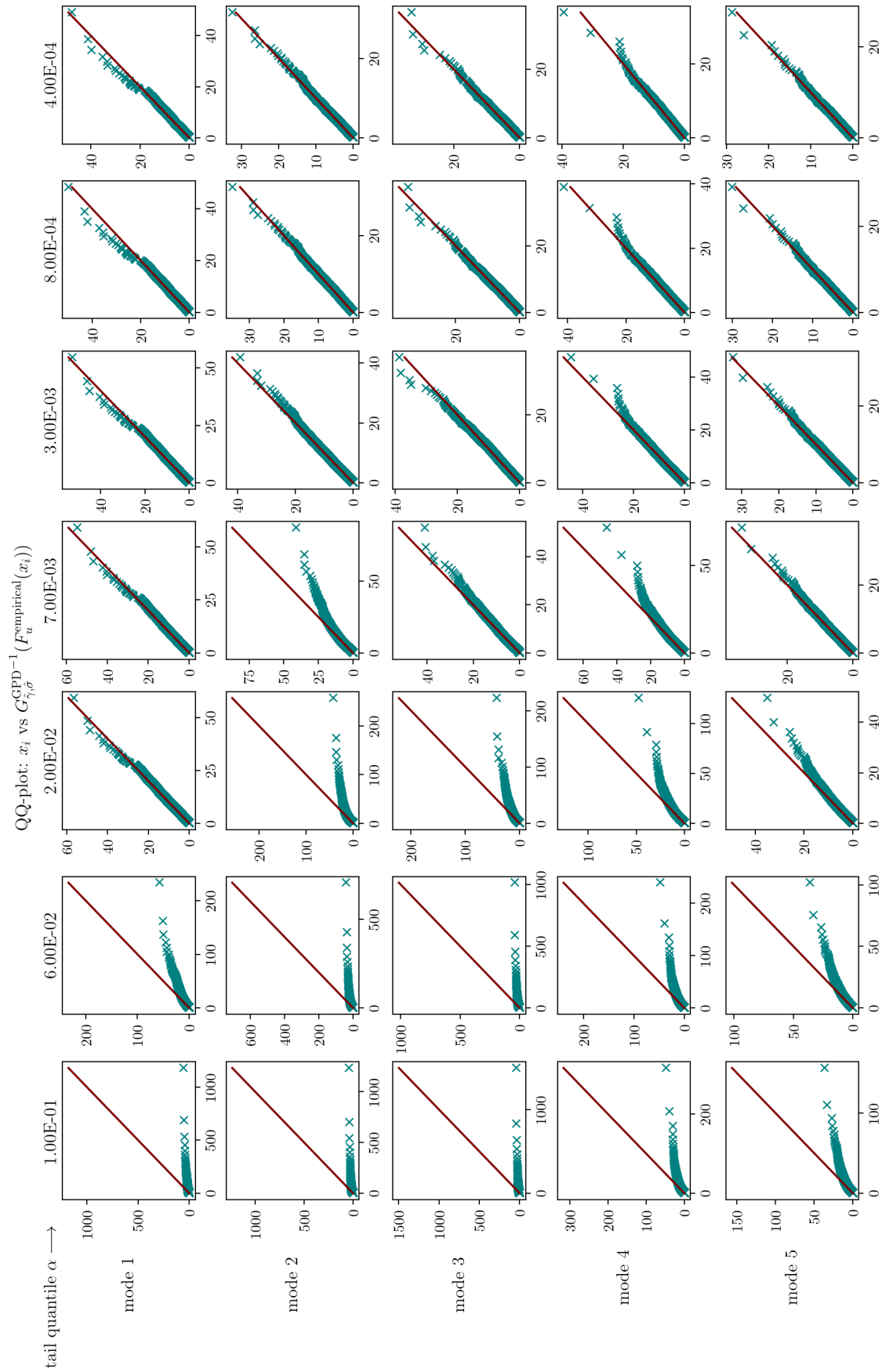


Figure 24: Q-Q plots of fitted GPD with increasing threshold, negative tail.

## A.2.2 Residual/Local Threshold Fit

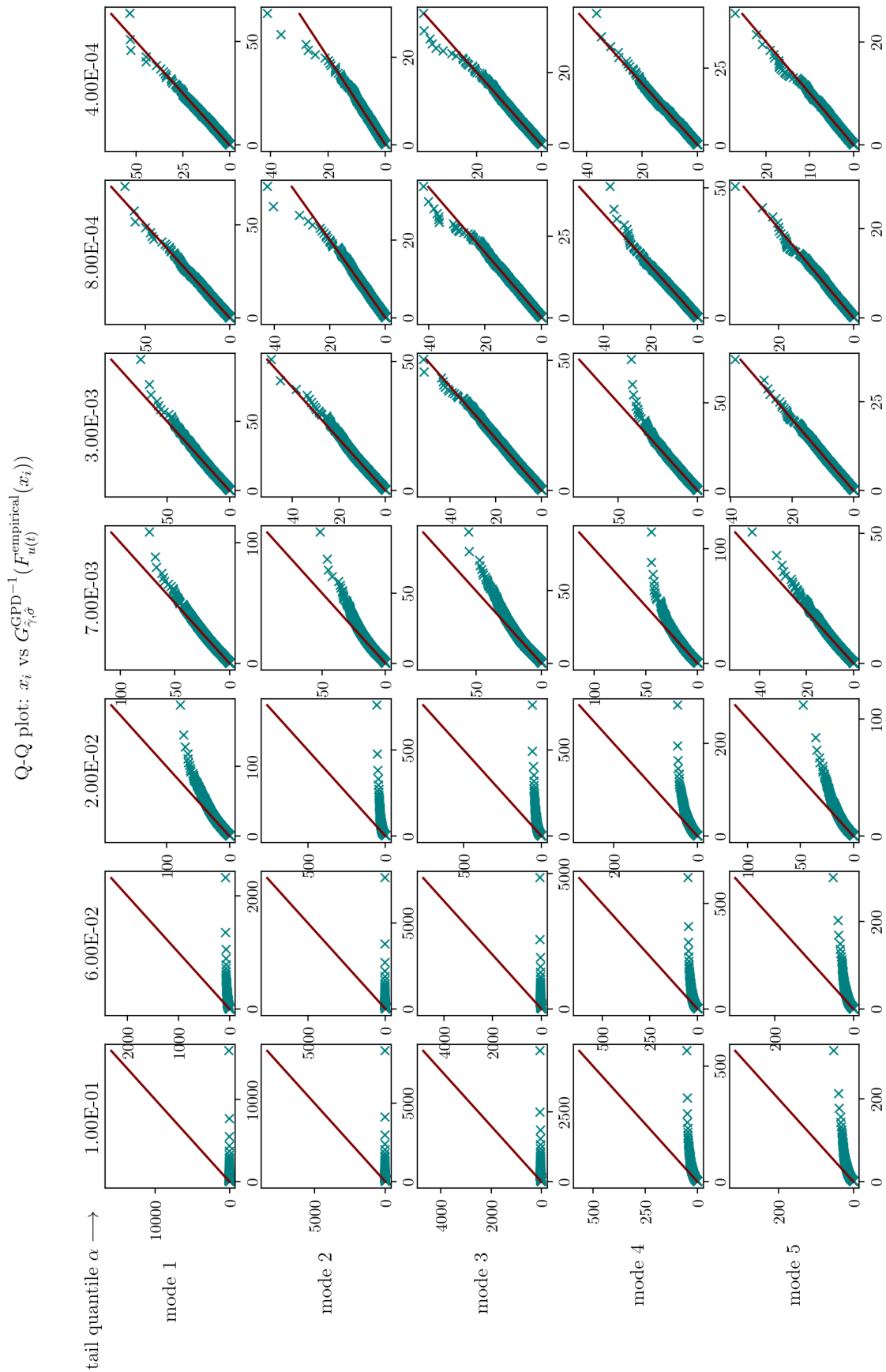


Figure 25: Q-Q plots of fitted GPD with increasing local tail-quantile threshold, positive tail.